RadioGraphics

Diffusion-weighted Imaging of the Breast: Principles and Clinical Applications[1]

TEACHING POINTS
See last page

Reiko Woodhams, MD, PhD • Saadallah Ramadan, PhD • Peter Stanwell, PhD • Satoko Sakamoto, MD • Hirofumi Hata, RT • Masanori Ozaki, RT Shinichi Kan, MD, PhD • Yusuke Inoue, MD, PhD

Diffusion-weighted imaging provides a novel contrast mechanism in magnetic resonance (MR) imaging and has a high sensitivity in the detection of changes in the local biologic environment. A significant advantage of diffusion-weighted MR imaging over conventional contrast material–enhanced MR imaging is its high sensitivity to change in the microscopic cellular environment without the need for intravenous contrast material injection. Approaches to the assessment of diffusion-weighted breast imaging findings include assessment of these data alone and interpretation of the data in conjunction with T2-weighted imaging findings. In addition, the analysis of apparent diffusion coefficient (ADC) value can be undertaken either in isolation or in combination with diffusion-weighted and T2-weighted imaging. Most previous studies have evaluated ADC value alone; however, overlap in the ADC values of malignant and benign disease has been observed. This overlap may be partly due to selection of *b* value, which can influence the concomitant effect of perfusion and emphasize the contribution of multicomponent model influences. The simultaneous assessment of diffusion-weighted and T2-weighted imaging data and ADC value has the potential to improve specificity. In addition, the use of diffusion-weighted imaging in a standard breast MR imaging protocol may heighten sensitivity and thereby improve diagnostic accuracy. Standardization of diffusion-weighted imaging parameters is needed to allow comparison of multicenter studies and assessment of the clinical utility of diffusion-weighted imaging and ADC values in breast evaluation. Supplemental material available at *http://radiographics.rsna.org/lookup/suppl/doi:10.1148/rg.314105160/-/DC1*.

Abbreviations: ADC = apparent diffusion coefficient, ASSET = array spatial sensitivity encoding technique, DCIS = ductal carcinoma in situ, FOV = field of view, IDC = invasive ductal carcinoma, RARE = rapid acquisition with relaxation enhancement, RF = radiofrequency, SNR = signal-to-noise ratio, SpecIR = spectrally selected inversion recovery, SSRF = spatial-spectral radiofrequency, STIR = short inversion time inversion recovery, TE = echo time, TR = repetition time

RadioGraphics 2011; 31:1059–1084 • **Published online** 10.1148/rg.314105160 • **Content Codes:** BR OI MR PH

[1]From the Department of Diagnostic Radiology, Kitasato University School of Medicine and Kitasato University Hospital, 1-15-1 Kitasato, Minamiku, Sagamihara, Kanagawa 252-0375, Japan (R.W., S.S., H.H., M.O., S.K., Y.I.); Centre for Clinical Spectroscopy, Department of Radiology, Brigham and Women's Hospital, Harvard Medical School, Boston, Mass (S.R.); and Faculty of Health, University of Newcastle, Callaghan, NSW, Australia (P.S.). Recipient of a Certificate of Merit award for an education exhibit at the 2009 RSNA Annual Meeting. Received June 28, 2010; revision requested September 28; final revision received January 6, 2011; accepted January 10. All authors have no financial relationships to disclose. **Address correspondence to** R.W. (e-mail: *reikow@hotmail.co.jp*).

Introduction

Diffusion-weighted imaging is a modality that makes use of magnetic resonance (MR) imaging to depict the diffusivity of water molecules in a defined voxel by means of the application of motion-probing gradients. This imaging property is unique and provides a different contrast mechanism than that observed on conventional T1- and T2-weighted MR images. Evaluation of breast images acquired with sensitization to the diffusion of water molecules has the potential to play an adjunct role in the assessment of breast tissue.

Diffusion-weighted imaging was initially applied in the clinical setting in the mid-1990s for the diagnosis of acute stroke. At that time, diffusion-weighted imaging demonstrated a high diagnostic utility, not only in the investigation of acute stroke, but also in developing the differential diagnosis for other brain abnormalities, including tumors and abscesses. Subsequent technical advances in MR imaging, including the development of ultrafast imaging sequences and the proliferation of array coils and of imagers with higher magnetic field strength (which increase signal-to-noise ratio [SNR] per unit time) have led to a reduction in the impact of motion artifacts and the investigation of organs other than the brain. Diffusion-weighted imaging has subsequently been used in the evaluation of disease processes in various anatomic locations (eg, chest, liver, pancreas, prostate gland) that had previously not been studied due to difficulties resulting from movement during patient respiration, peristalsis, and low inherent SNR (1).

In 1997, Englander et al (2) addressed the possibility of applying diffusion-weighted imaging to the human breast. Since that time, clinical studies have been undertaken, and several studies have shown diffusion-weighted imaging to be highly sensitive for the evaluation of breast cancer and a possible means of differentiating between benign and malignant tumors (3–10). As a result of these findings, diffusion-weighted breast imaging has attracted greater interest among breast imagers, with many clinicians advocating applications beyond just clinical research. However, the incorporation into clinical decision making of information gleaned from diffusion-weighted breast imaging has been slow compared to the use of information obtained from diffusion-weighted imaging of other organs. One reason is that the diagnostic role of diffusion-weighted imaging in breast imaging has not been incorporated into the already established Breast Imaging and Reporting Data System lexicon (11). Contrast material–enhanced breast MR imaging is currently accepted as the most sensitive imaging technique for the diagnosis and staging of breast cancer. However, several studies have noted that conventional breast MR imaging, including T2-weighted imaging and contrast-enhanced T1-weighted imaging, is limited in terms of specificity in the assessment of breast tumors (12–14). Consequently, there has been considerable interest in the development of adjunct MR imaging methods to improve the specificity of dynamic contrast-enhanced breast MR imaging, and diffusion-weighted breast imaging is being investigated for its potential to improve breast disease diagnosis at the cost of a small increase in examination time.

In this article, we discuss the principles of diffusion-weighted imaging, offer suggestions for optimizing diffusion-weighted breast imaging technique, and discuss the clinical implementation of diffusion-weighted breast imaging.

Principles of Diffusion-weighted Imaging

Proton Diffusion in Biologic Tissue

Diffusion is the random and thermal (Brownian) motion of water molecules (or any other type of molecule). This motion is affected by the local tissue environment and the presence of barriers (eg, cell membranes and semipermeable membranes). The motion of water molecules is more restricted in tissues with a high cellular density (eg, tumor tissue) or with lipophilic cell membranes acting as barriers in both the extracellular and intracellular spaces. In contrast, the motion of water molecules is less restricted in areas of low cellularity or where cell membranes have been destroyed. A less cellular environment provides a larger extracellular space for the diffusion of water molecules, which may also freely transgress defective cell membranes to move from the extracellular into the intracellular compartment. Therefore, the degree of water diffusion in tissue is inversely correlated with tissue cellularity and the integrity of cell membranes. Diffusion-weighted imaging is used to visualize the degree of water molecule diffusion at in vivo MR imaging. Signal intensity at diffusion-weighted imaging is inversely proportional to the degree of water molecule diffusion, which will be influenced by the histologic structure; in other words, the signal intensity will imply the histologic structure.

Teaching Point

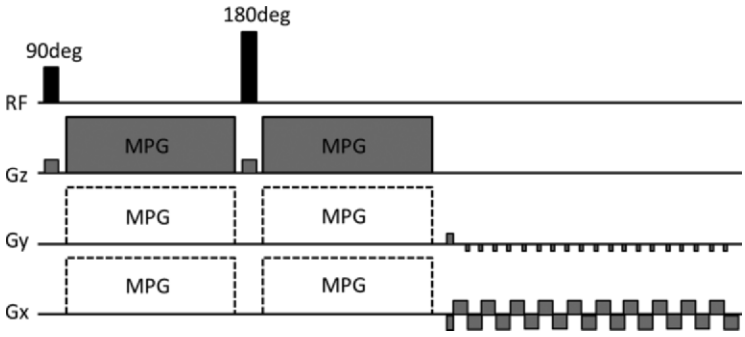

Figure 1. Graph illustrates the pulse sequence of single-shot spin-echo echoplanar diffusion-weighted imaging. *G* = gradient, *MPG* = motion-probing gradient.

Diffusion is quantified by measuring what is known as the apparent diffusion coefficient (ADC) value in square millimeters per second, which defines the average area covered by a molecule per unit time. The ADC value can be calculated by assessing the signal attenuation that occurs at diffusion-weighted imaging performed at different *b* values.

Technical Considerations

Spin-echo echoplanar diffusion-weighted imaging is the most popular clinical technique for generating diffusion-weighted images. To introduce diffusion weighting into a spin-echo echoplanar imaging sequence, two diffusion-sensitizing gradients are "sandwiched" around a 180° radiofrequency (RF) refocusing pulse before echoplanar imaging data collection (Fig 1). Diffusion can be expressed as the following monoexponential equation:

$$\ln(S_{DW}/S_{SE}) = \mathrm{ADC}(\gamma \cdot G \cdot \delta)^2 \times (\Delta - [\delta/3]), \quad (1)$$

where G is the gradient, S_{DW} is the attenuated spin-echo signal (G = 0), S_{SE} is the full spin-echo signal without diffusion attenuation (G = 0), γ is the proton gyromagnetic ratio, δ is the duration of G, and Δ is the time delay between the leading edges of the two diffusion-sensitizing gradients. The product of the last two terms in Equation 1—that is, $(\gamma \cdot G \cdot \delta)^2 \times (\Delta - [\delta/3])$—is usually known as the *b* value (expressed in seconds per square millimeter) and represents the strength of diffusion weighting.

The faster a molecule diffuses, the greater the attenuation and the weaker the corresponding pixel signal intensity at diffusion-weighted imaging. Thus, signal intensity is usually higher in a region with restricted diffusion than in a region with fast diffusion. As a reference point, the ADC value of free water molecules at 37°C is 3.0×10^{-3} mm²/sec.

ADC Value

The ADC value is a quantitative measurement of diffusion that is calculated on the basis of the attenuation in signal intensity between at least two diffusion-weighted images according to the following equation:

$$\text{ADC value} = -\ln(S_{DW}/S_{SE})/b, \quad (2)$$

where S_{DW} is the attenuated spin-echo signal and S_{SE} is the full spin-echo signal without diffusion attenuation. A low ADC value indicates restricted proton diffusion, which typifies malignant tissue. In vivo, the measured ADC value includes the factors of both water diffusion and perfusion effect; hence the term *apparent* diffusion coefficient:

$$\text{ADC value} \approx D + (f/b), \quad (3)$$

where *D* = diffusion coefficient and *f* = perfusion factor.

In living tissue, diffusion-weighted imaging is affected by Brownian incoherent motion (diffusion) and microperfusion or blood flow. Microperfusion, defined as the microcirculation of body fluids assumed to stay within the capillary network, is an important potential competitor with the previously defined diffusion phenomenon. This means that the diffusion-weighted imaging signal can be mixed with a perfusion signal, thus increasing the net ADC value according to Equation 3. Use of a higher *b* value reduces the contribution of perfusion effects in ADC measurements according to Equation 3. The "*f*/*b*" factor can be ignored with higher *b* values because *f* generally consists of only a few percentage points. Microperfusion effect has not been observed at a *b* value of less than 600 sec/mm² in normal fibroglandular breast tissue or in adipose tissue, a finding that is consistent with

reports that the mammary gland is not a highly vascular organ (15,16). However, the fact that microperfusion is high in both benign and malignant lesions is common knowledge in the scientific community (17).

The observed ADC value depends on many factors, including fluid viscosity, membrane permeability effecting intracellular-extracellular water exchange, water transport mechanisms, and the structural design of the compartment containing diffusing water. Thus, it is evident that ADC value can provide a specific type of information not otherwise available.

An ADC map is a parametric image whose color scale or gray scale represents the ADC values of the voxels and is usually generated by proprietary or third-party software.

ADC measurements obtained in almost every organ in the body have been reported (18–23), including in the breast, where ADC values in various disease states have been compared (3–8,24–29).

Suggestions for Optimal Imaging

Echoplanar diffusion-weighted imaging can result in image distortion due to eddy currents, susceptibility effects, and ghosting artifacts that occur during data acquisition. It is recommended that the MR imaging operator follow standard procedures to optimize image acquisition parameters and reduce artifacts before embarking on a diffusion-weighted imaging study. Suggestions related to the acquisition of diffusion-weighted images are summarized in Table 1. The choice of number of phase-encoding steps and other spatial resolution–enhancing guidelines are the same as for routine MR imaging procedures.

Echoplanar Imaging versus Other Techniques

Baltzer et al (30) conducted a study comparing echoplanar diffusion-weighted imaging with half-Fourier rapid acquisition with relaxation enhancement (RARE) diffusion-weighted imaging in terms of lesion visibility, ADC value, and tumor size estimation. Their study revealed a higher sensitivity for echoplanar diffusion-weighted imaging, a higher specificity for half-Fourier RARE diffusion-weighted imaging, and statistically similar ADC values with both techniques. They also reported that half-Fourier RARE diffusion-weighted imaging produced a lower SNR with fewer image artifacts, whereas more image artifacts and a higher SNR were associated with echoplanar diffusion-weighted imaging.

Table 1
Suggestions for Optimal Diffusion-weighted Imaging

Perform slab shimming to reduce B_0 inhomogeneities
Use spin-echo echoplanar imaging rather than gradient-echo echoplanar imaging, which is more sensitive to B_0 inhomogeneities; better still, use segmented spin-echo echoplanar imaging because it is much less sensitive to off-resonance artifacts
Reduce the number of k-space lines read per single excitation (I factor)
Optimize bandwidth value to allow minimum echo spacing; bandwidth must be increased to reduce chemical shift artifact, since low bandwidth causes image distortions in the phase-encoding direction
Enable fat saturation

Selection of Fat Suppression Technique

For the acquisition of diffusion-weighted breast images, suppression of lipid signal is essential to reduce image artifacts (eg, ghosting, chemical shift artifact) and increase lesion conspicuity. There are two common approaches to lipid suppression in diffusion-weighted breast imaging: *(a)* spectral fat suppression, in which a spatial-spectral radiofrequency (SSRF) prepulse is applied before the echoplanar diffusion-weighted sequence; and *(b)* inversion recovery, in which a 180° RF prepulse with short inversion time inversion recovery (STIR) is applied prior to performing the echoplanar diffusion-weighted sequence. Generally, fat suppression will provide better SNR than will STIR. However, STIR provides more homogeneous fat suppression than does a fat suppression technique.

Wenkel et al (31) compared these two fat suppression techniques in a diffusion-weighted breast imaging study performed at 1.5 T with an inversion time of 190 ms, and found that *(a)* the ADC value was significantly different between these two techniques, and *(b)* there was a larger overlap in the ADC values of benign and malignant tumors with STIR than with fat suppression. In addition, lesion delineation was better with fat suppression than with STIR, possibly due to improved SNR per unit time with fat suppression.

Baron et al (16) conducted another study in which four types of fat suppression were compared at 1.5 T: STIR, fat saturation, spectrally adiabatic inversion recovery, and water excitation. Small differences between ADC values were observed at lower *b* values, with larger differences at higher *b* values. Of the four techniques, water excitation was found to yield the highest SNR (16).

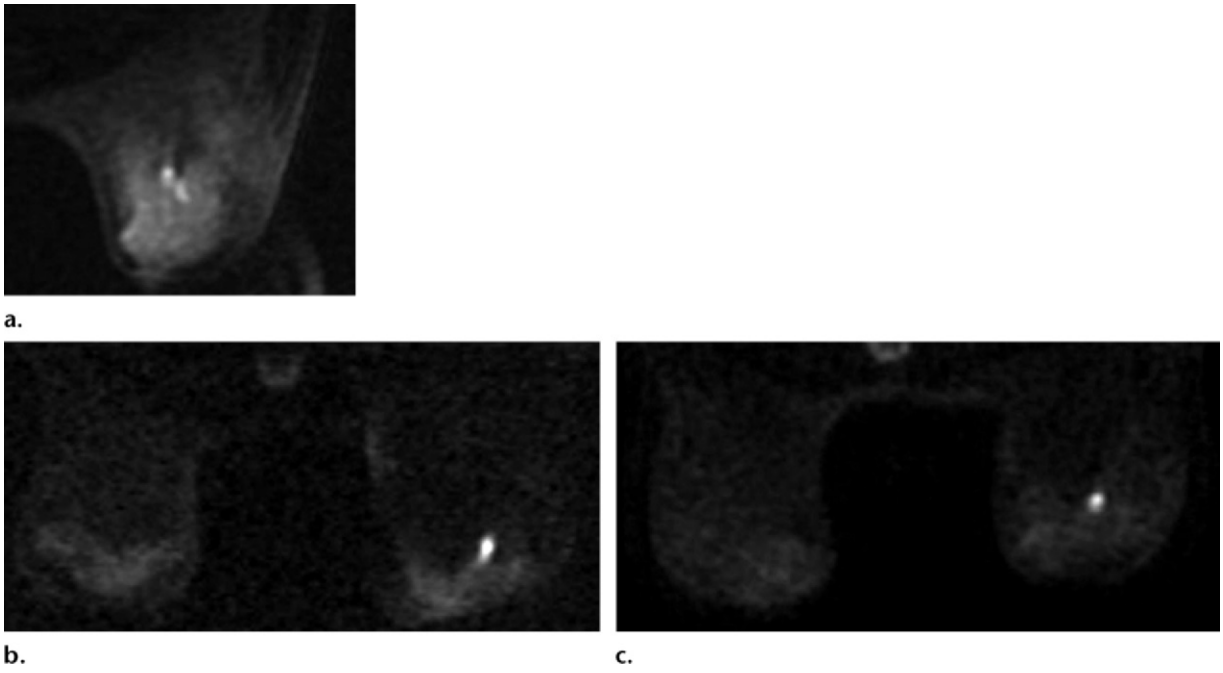

Figure 2. DCIS as measured in a patient over a 5-year period. The patient had undergone ultrasonography-guided biopsy several times, which resulted in benign histologic findings over the entire period. All MR images were acquired at 1.5 T. **(a)** Diffusion-weighted MR image obtained in 2005 at b = 750 sec/mm^2 without ASSET using a single-channel coil (spin-echo echoplanar imaging, repetition time [TR] msec/echo time [TE] msec = 6000/68.3, bandwidth = ±129 kHz, field of view [FOV] aspect ratio = 0.8 [320 × 256], matrix = 128 × 128, section thickness = 6 mm, no intersection gap, SSRF prepulse). **(b)** Diffusion-weighted MR image obtained in 2008 at b = 1500 sec/mm^2 without ASSET (spin-echo echoplanar imaging, TR/TE = 8200/75.3, bandwidth = ±250 kHz, FOV aspect ratio = 0.7 [340 × 238], matrix = 160 × 192, section thickness = 5 mm, no intersection gap, SSRF prepulse). **(c)** Diffusion-weighted MR image obtained in 2009 at b = 1500 sec/mm^2 with ASSET (spin-echo echoplanar imaging, TR/TE = 7800/88.4, bandwidth = ±250 kHz, FOV = 340 mm, matrix = 160 × 192, section thickness = 5 mm, no intersection gap, SSRF prepulse) shows improved SNR and reduced image artifacts.

In contrast, Kazama et al (32) found that the ADC values obtained using STIR and fat-suppressed diffusion-weighted imaging techniques at 1.5 T were very similar, and that STIR diffusion-weighted imaging–based methods provided more homogeneous fat suppression.

In summary, STIR has the disadvantage of decreased SNR and potential overlap of ADC values, whereas fat suppression technique suffers from inhomogeneous suppression of fat.

Application of Parallel MR Imaging

Parallel MR imaging, a newer technique that is increasingly being used, makes use of spatial encoding from multiple RF detector coils to supplement the encoding supplied by magnetic field gradients, thereby making MR image acquisition time shorter than what was possible previously. To reduce acquisition time, a certain fraction of phase-encoding steps are skipped, resulting in a sparsely sampled k-space matrix. This is accomplished by using the spatial information contained in an array of RF coils in combination with a special reconstruction strategy.

The benefits of parallel MR imaging are greatest with single-shot sequences (eg, echoplanar imaging sequences) due to reduced relaxation effects of the signal and, therefore, reduced blurring and other artifacts (33). In addition, the combination of single-shot sequences and parallel MR imaging can be used to reduce effective interecho spacing, ultimately resulting in decreased image distortion. Several studies have shown the advantages of using parallel MR imaging for diffusion-weighted breast imaging studies. In one study, the sensitivity-encoding technique (34) was used, resulting in a reduction in the number of phase-encoding steps and in acquisition time, with an associated reduction in susceptibility and chemical shift artifacts (3). Similarly, in another study, in which diffusion-weighted breast imaging with the proprietary array spatial sensitivity encoding technique (ASSET; GE Healthcare, Waukesha, Wis) was used, there was a reduction in image distortion, susceptibility artifacts, and acquisition time relative to other methods (Fig 2) (17).

Use of Breast Coils

A wide variety of commercially manufactured breast coils are currently available for breast imaging, many of which incorporate multichannel coils that allow parallel imaging techniques, thereby shortening imaging time by reducing the number of phase-encoding steps and reducing image distortion in echoplanar techniques. When a sufficient number of coil elements are arranged in the phase-encoding direction, time can be saved by reducing the number of phase-encoding steps required to complete k-space filling. For optimal and effective use of parallel imaging, there must be a sufficient number of coil elements arranged in the phase-encoding direction to reduce the number of phase-encoding steps. Reduction in imaging time, commonly referred to as the acceleration factor, is a function of the number of coil elements and their arrangement in the phase-encoding direction. As a result of time reduction and the elimination of some phase-encoding steps, SNR is also reduced. This reduction in SNR can sometimes be overcome by increasing the number of signal acquisitions or by increasing phase oversampling. Single-shot techniques (eg, echoplanar imaging) in particular can benefit from the use of parallel imaging for reduction of image artifacts.

Table 2
Parameters for Single-Shot Echoplanar Diffusion-weighted Imaging at 1.5 T with a Dedicated Eight-Channel Breast Coil

Parameter	Specification
b value (sec/mm²)	0, 1000; 0, 1500
TR/TE (msec)	7800/80,† 7800/88†
Fat suppression	SSRF prepulse
FOV (mm)	340
Matrix	160 × 192
Section thickness (mm)	5
Intersection interval (mm)	0
MPG	3
No. of signals averaged	4 (*b* = 1000 sec/mm²), 6 (*b* = 1500 sec/mm²)
rBW (kHz)	±125
ASSET	Yes
Imaging time (min)	5

Note.—MPG = motion-probing gradient, rBW = receiver bandwidth.
*MR imager (HDx) and breast coil manufactured by GE Medical Systems, Waukesha, Wis.
†Minimum TE is automatically determined.

Diffusion-weighted Breast Imaging in Clinical Practice

Diffusion-weighted breast imaging is technically challenging for several reasons: *(a)* the breast tissue is off center within the imager bore, *(b)* there are inherent susceptibility artifacts due to the presence of air surrounding the breast and the proximity of the adjacent air-filled thorax, *(c)* the breast has an irregular shape, and *(d)* the breast contains abundant fat tissue. However, many technical improvements can be used to improve image quality in diffusion-weighted imaging for breast disease.

The introduction of diffusion-weighted imaging into routine clinical evaluation of breast disease requires attention to some important points.

1. Patient position is crucial to the final quality of diffusion-weighted breast images. Both breasts have to fit entirely within the coil. Positioning pads and cushions should be used to eliminate skin folds within the coil, near the axilla, and under the breast (eg, abdominal fat). Skin folds may cause inhomogeneous fat suppression that will affect image quality.

2. Shimming and uniform fat suppression. Shimming is used to reduce magnetic field inhomogeneities across the volume of the FOV. On some commercial imagers, shimming can be selected to be automatically performed before diffusion-weighted image acquisition, after which the operator has the option of manually adjusting and improving the automated shim. Shimming is important in echoplanar diffusion-weighted imaging because it contributes to more effective and homogeneous fat suppression. Improved shimming, or a higher magnetic field strength, allows better spectral separation of water and fat resonances (224 Hz at 1.5 T and 448 Hz at 3 T), and thus, better fat suppression. Table 2 shows the acquisition parameters for our diffusion-weighted imaging sequence as performed at 1.5 T. Diffusion-weighted imaging is performed prior to contrast enhancement to avoid the effect of contrast material.

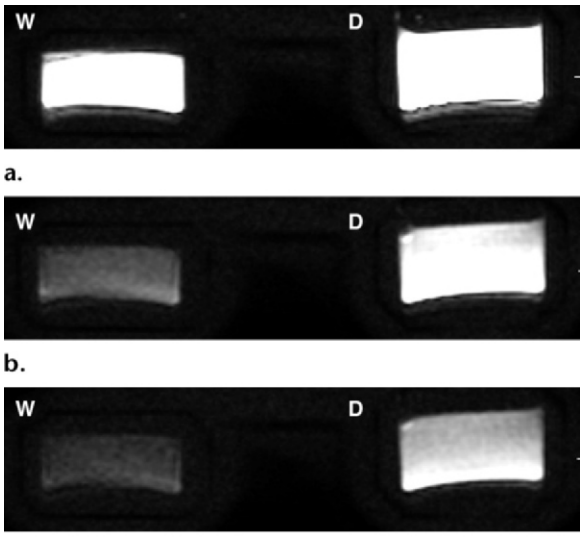

Figure 3. Diffusion-weighted images of a phantom, obtained at *b* values of 1000 **(a)**, 1750 **(b)**, and 2000 **(c)** sec/mm², show how the signal intensity of water *(W)* and detergent *(D)* decreases as *b* value increases. The signal intensity of detergent remains high until $b = 1750$ sec/mm², whereas the signal intensity of water is close to the noise level at $b = 2000$ sec/mm². This is because detergent has a higher viscosity than water.

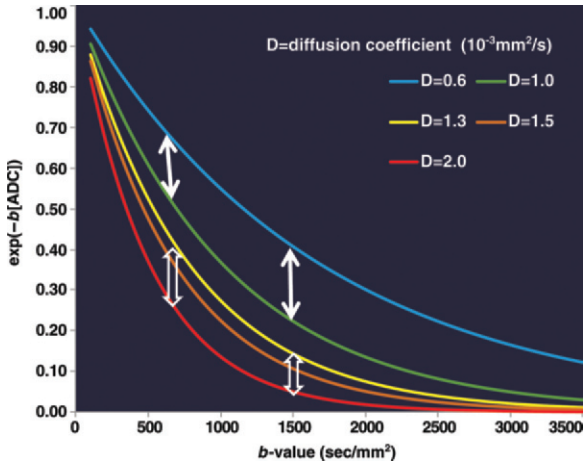

Figure 4. Graph illustrates the correlation between $\exp(-b \cdot D)$ and *b* value at various diffusion coefficients. According to Equation 4, $\exp(-b \cdot D)$ is proportional to the signal intensity at diffusion-weighted imaging. Arrows indicate the signal contrast between different tissue types with various diffusion coefficients. Higher signal contrast can be seen between lower diffusion coefficients at a higher *b* value than at a lower *b* value (solid arrows). On the other hand, higher signal contrast can be seen between higher diffusion coefficients at a lower *b* value than at a higher *b* value (open arrows).

Correlation between Signal Intensity, *b* Value, and ADC Value

Signal Intensity and *b* Value

Signal intensity at diffusion-weighted imaging is influenced by *b* value according to the following equation, which is modified from Equation 1:

$$S_{DW} = S_{SE}(\exp[-b \cdot D]) \propto \rho(1 - \exp[-TR/T1]) \times \exp(-TE/T2) \times \exp(-b \cdot D), \quad (4)$$

where *D* is the diffusion coefficient, S_{DW} is the attenuated spin-echo signal, S_{SE} is the full spin-echo signal without diffusion attenuation, and ρ is the spin density (35,36). According to this equation, the signal intensity at diffusion-weighted imaging consists of T2-weighted signal and diffusion-weighted signal. The latter is emphasized with the application of higher motion-probing gradients. On the other hand, T2-weighted signal will be emphasized at lower *b* values (T2 shine-through effect). In addition, the signal intensity at diffusion-weighted imaging will decrease as *b* value increases; thus, an SNR that is sufficient for lesion detection must be provided while emphasizing the contribution from the diffusion coefficient alone because of their "trade-off" relationship (Fig 3).

In Equation 4, $(1 - \exp[-TR/T1])$ is approximately 1, since TR is much greater than T1 for single-shot spin-echo echoplanar imaging. Therefore, Equation 4 can be rewritten as follows:

$$S_{DW} \propto \rho\ (\exp[-TE/T2]) \times \exp(-b \cdot D). \quad (5)$$

Figure 4 is a graph of $\exp(-b \cdot D)$, which is proportional to signal intensity at diffusion-weighted imaging (S_{DW}) (see Eq 4), versus *b* value. In this case, the signal intensity at T2-weighted imaging is determined to be consistent. The signal intensity at diffusion-weighted imaging becomes lower as *b* value increases, but a higher *b* value emphasizes contrast resolution between various diseases and normal breast tissue. However, an overly high *b* value reduces the overall SNR of the experiment.

Teaching Point

Identification of a discrete breast lesion is mandatory for evaluating its ADC value, and doing so requires sufficient contrast resolution to

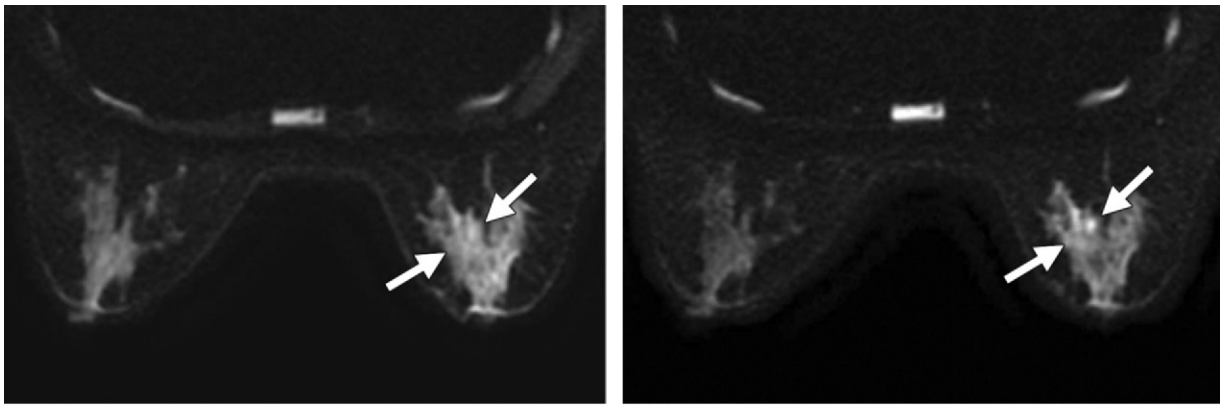

a. b.

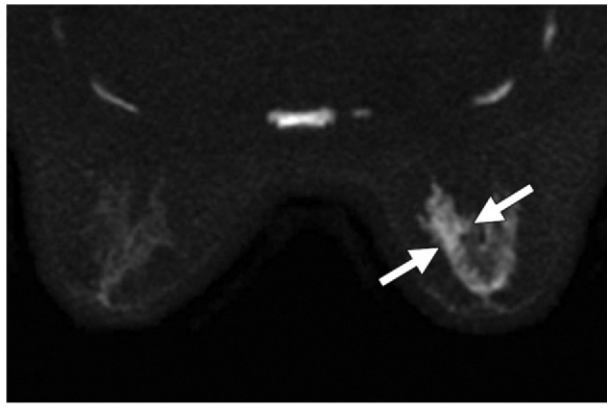

c.

Figure 5. Ductal carcinoma in situ (DCIS) in the left breast. Diffusion-weighted images obtained at *b* values of 500 **(a)**, 1000 **(b)**, and 1500 **(c)** sec/mm² show that the signal intensity of normal breast parenchyma decreases with increasing *b* value. The signal intensity of DCIS in the right breast (arrows) is conspicuous relative to the decreased signal intensity of normal breast parenchyma in **b**, and the signal intensity of normal breast parenchyma in the left breast is close to the noise level in **c**.

differentiate the breast lesion from the adjacent breast parenchyma. Kuroki and Nasu (9) compared the signal intensity of the normal mammary gland with that of breast cancer at various *b* values to establish the optimal *b* value. In their study, a *b* value of 1000 sec/mm² was considered optimal for diffusion-weighted breast imaging, since the signal of the normal mammary gland is suppressed and the signal of breast cancer is sufficiently high to allow detection and evaluation. On the other hand, the authors stated that the signal of the mammary gland might not be suppressed at $b = 1000$ sec/mm² in cases of severe fibrocystic disease (9), and recent studies have documented the usefulness of a *b* value of 1500 sec/mm² (10,37,38). Figure 5 illustrates signal attenuation in a normal mammary gland and breast cancer at various *b* values. Although the use of higher *b* values has been advocated for diffusion-weighted brain imaging to obtain better contrast between normal tissue and ischemic areas (39,40), such results are not likely in the breast. The use of higher *b* values may be ideal for the evaluation of dense breast tissue; however, the evaluation of small lesions (including DCIS) may be hampered at high *b* values due to more rapid signal decay. Pereira et al (41) analyzed the ADC values of breast cancers at *b* values ranging from 0 to 1000 sec/mm² and found that the ADC value calculated for a combination of *b* values of 0 and 750 sec/mm² showed a slightly better sensitivity and specificity than did the ADC value calculated for other *b*-value combinations. The optimal *b* value for diffusion-weighted breast imaging remains controversial, since the optimal *b* value required for visual interpretation may differ from that required for ADC value analysis. Table 3 summarizes the effect of *b* value on the visibility of breast lesions.

b Value and ADC Value

ADC value may be more specific than signal intensity change at diffusion-weighted imaging alone. However, at low *b* values, the ADC value is influenced by tissue microperfusion, resulting in a higher value. The microperfusion effect has been observed in the parotid gland ($b < 500$ sec/mm²), abdominal organs ($b < 300$ sec/mm²), bone marrow ($b < 200$ sec/mm²), skeletal muscle ($b < 60$ sec/mm²), and human placenta ($b < 50$ sec/mm²) (42–45). The microperfusion effect in normal fibroglandular breast tissue is not considered significant

Table 3
Effect of *b* Value on the Visibility of Breast Lesions

b Value (sec/mm²)	Quality	SNR, CNR	Conspicuity Against the Breast Parenchyma	Visual Differentiation Between Benign and Malignant Lesions	Benign Tumor	Low-Grade DCIS	High-Grade DCIS, IDC
1000	++	+++	+	+	++	++	+++
1500	++	++	++	++	+	+	+++

Note.—CNR = contrast-to-noise ratio, IDC = invasive ductal carcinoma, +++ = excellent, ++ = good, + = acceptable.

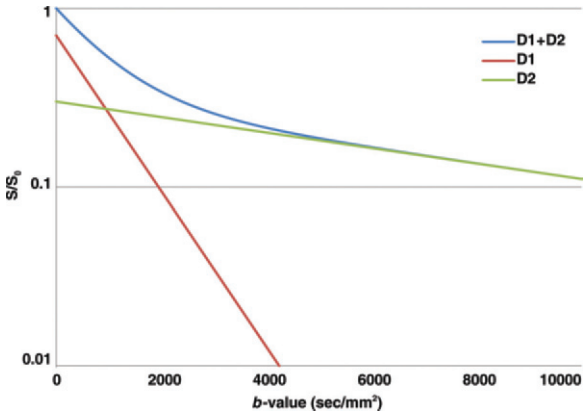

Figure 6. Simulations of single-compartment and two-compartment models with extracellular free diffusion and intracellular restricted diffusion. Graph illustrates the correlation between S/S_0 (S = signal intensity with diffusion, S_0 = signal intensity without diffusion) and b value, expressed as $S/S_0 = f_1(\exp[-b \cdot D_1]) + f_2(\exp[-b \cdot D_2])$, where D_1 = extracellular diffusion coefficient, D_2 = intracellular diffusion coefficient, f_1 = extracellular volume fraction, and f_2 = intracellular volume fraction. Parameters were as follows: $D_1 = 1.0 \times 10^{-3}$ mm²/sec, $D_2 = 0.1 \times 10^{-3}$ mm²/sec, $f_1 = 0.7$, and $f_2 = 0.3$.

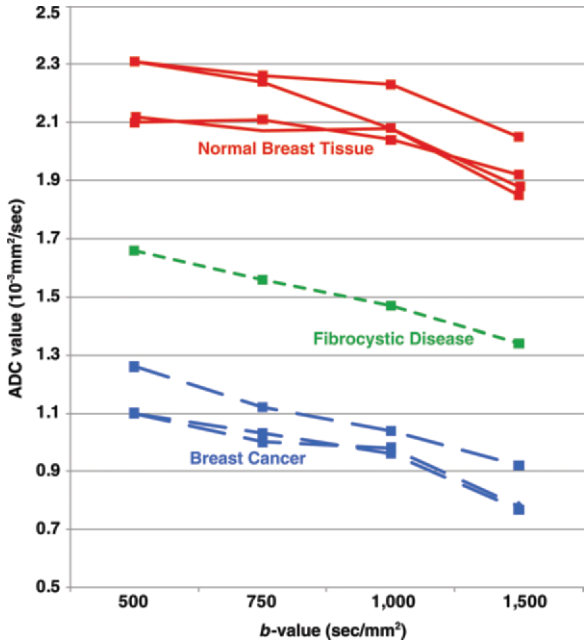

Figure 7. Changes in ADC value versus changes in *b* value. Diffusion-weighted images were obtained at *b* values of 500, 750, 1000, and 1500 sec/mm², and the ADC value at each *b* value was calculated from the signal intensity of diffusion-weighted images obtained at each *b* value and at $b = 0$ sec/mm². All cases show a decrease in ADC value with an increase in *b* value.

because of the low vascularity of breast tissue (16). However, this effect could be more pronounced in breast cancer because of increased vascularity, although this has not yet been proved.

Recent studies have documented that the signal decay fits the multiexponential model in vivo at higher *b* values, in which each compartment has different ADC values. The simplest model is the intracellular-extracellular compartments model, which is applied to the brain and prostate gland (Fig 6) (42,46). The important point is that ADC values can be influenced by which *b* values are applied, a fact that highlights the need for consistent and standardized protocols. Figure 7 illustrates the decrease in ADC value with a change in *b* value in various diseases.

Teaching Point

Pereira et al (41) analyzed the ADC values of benign and malignant breast tumors with various combinations of *b* values (0, 250, 500, 750, and 1000 sec/mm²). They found that it is not necessary to use multiple *b* values because the sensitivity of an ADC value with two *b* values is equivalent to that with multiple *b* values. Given the time constraints of clinical practice, analysis of an ADC value with two *b* values may be considered reasonable and acceptable.

Table 4
Signal Intensity and ADC Value for Various Pathologic Conditions of the Breast

Pathologic Condition	Signal Intensity at Diffusion-weighted Imaging*	Signal Intensity at T2-weighted Imaging	ADC Value	Interpretation of Findings
Cancer, intraductal papilloma, abscess	High	Intermediate	Decreased	High-cellularity tumor, fibrous tissue with high water content
Bloody cyst, abscess	High	Intermediate to high	Decreased	Hemorrhage, high-viscosity fluid
Fibroadenoma, cyst, fibrocystic disease	Intermediate	Intermediate to high	Intermediate to high	Medium cellularity, high water content, proteinaceous fluid
Cyst, fibroadenoma, mucinous carcinoma	Low	High	Increased	High water content, low cellularity
Fibroadenoma, central necrosis of cancer, calcification, chronic hemorrhage	Low	Low	Decreased	Calcification, fibrous tissue with low water content, hyalinization, hemosiderin

*b = 1500 sec/mm^2. However, signal intensity may differ depending on the imaging parameters.

Signal Intensity and ADC Value

As described earlier, the high signal intensity on diffusion-weighted images reflects the restricted diffusion of water molecules in malignant tissue with high cellularity. Previous studies have shown an inverse correlation between the cellularity of breast cancer and ADC value (4,10,47). However, some benign breast tumors (eg, intraductal papilloma) may also have high cellularity and, consequently, a low ADC value. On the other hand, malignant disease with low cellularity (eg, DCIS) may demonstrate low signal intensity on diffusion-weighted images.

Tables E1 and E2 (online) summarize the parameters used for previous diffusion-weighted breast imaging studies and the findings obtained with these studies. Most of these studies demonstrated a significant difference in ADC value between benign and malignant tumors. Each article defines the cut-off point for the ADC value that provides high sensitivity and specificity for the discrimination of breast cancer (Table E2 [online]). However, there is overlap between benign and malignant diseases (10,37). Moreover, there is currently no standard ADC value for each breast disease because there is no consensus on an accepted range of b values for diffusion-weighted imaging. Several studies suggest the diagnostic assessment of diffusion-weighted images in combination with the assessment of signal intensity and lesion morphologic features on T2-weighted images (27,30). The combination of a high signal intensity at diffusion-weighted imaging, a low ADC value, an irregular margin, and iso- to hypointensity at T2-weighted imaging is a potential indication for malignancy. This combination method may improve the specificity of breast cancer assessment compared to a diagnosis made on the basis of ADC value alone (37). MR imaging consisting of a combination of diffusion-weighted and T2-weighted imaging and performed without the use of a gadolinium chelate may be a substitute for contrast-enhanced studies. Table 4 shows the signal intensities at diffusion-weighted imaging and T2-weighted imaging for various pathologic conditions of the breast.

Normal Breast Parenchyma.—Variation in the signal intensity and ADC value of normal breast parenchyma is observed due to normal hormonal

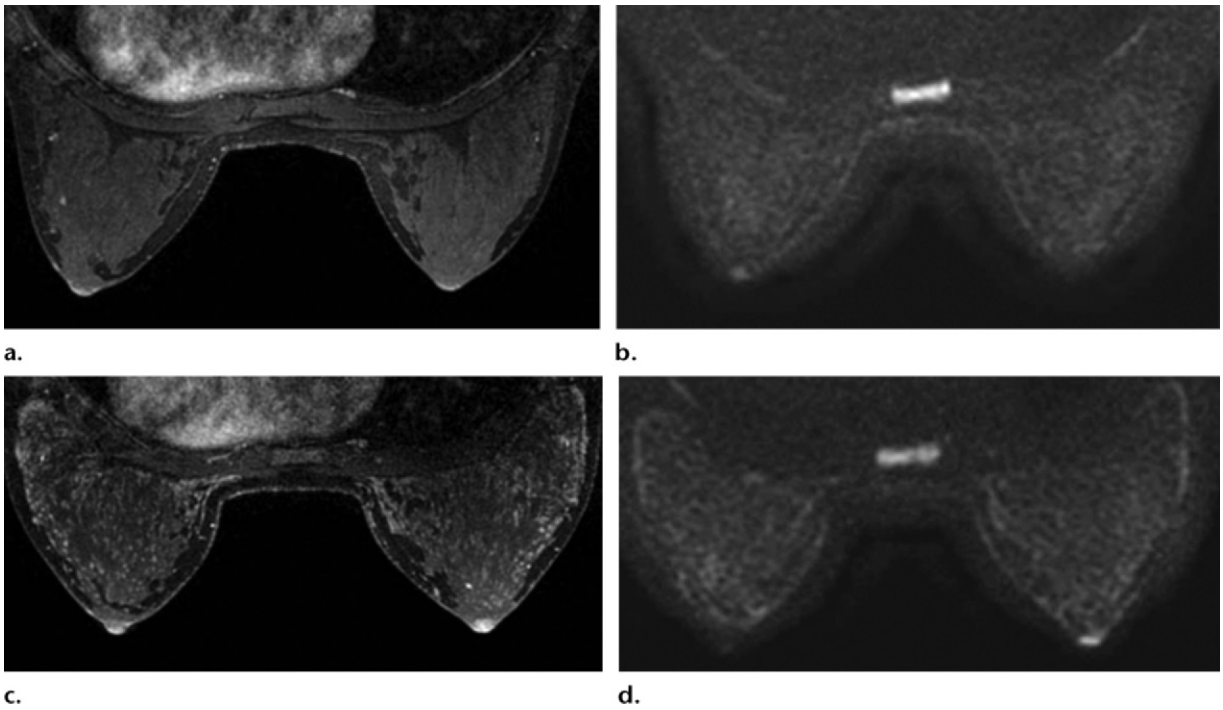

Figure 8. Changes in signal intensity and ADC value during the menstrual cycle in a 27-year-old woman. A focal asymmetric density was seen at mammography. **(a)** Contrast-enhanced T1-weighted MR image (VIBRANT [GE Healthcare], TR/TE = 6.5/3.1, flip angle = 12°, bandwidth = ±41.7 kHz, FOV = 360 mm, section thickness = 0.9 mm, no intersection gap, spectrally selected inversion recovery [SpecIR] with ASSET) obtained on day 22 of the menstrual cycle shows nonspecific punctate enhancement in both breasts. **(b)** On a diffusion-weighted image obtained at b = 1500 sec/mm^2 (spin-echo echoplanar imaging, TR/TE = 7800/88.4, bandwidth = ±250 kHz, FOV = 340 mm, matrix = 160 × 192, section thickness = 5 mm, no intersection gap, SSRF prepulse with ASSET) at the same time as **a**, no high-signal-intensity lesion is observed. **(c)** Contrast-enhanced T1-weighted MR image obtained on day 2 of the menstrual cycle shows diffuse contrast enhancement in both breasts. **(d)** On a diffusion-weighted image (b = 1500 sec/mm^2) obtained at the same time as **c**, slight diffuse nodular high signal intensity is observed in both breasts. The ADC value of breast tissue is higher on day 2 (2.26 × 10^{-3} mm^2/sec) than on day 22 (1.87 × 10^{-3} mm^2/sec).

fluctuations throughout the menstrual cycle and differences in individual physiologic and biochemical makeup (52). In women with normal menstrual cycles, ADC values decrease in week 2 and increase during week 4, although these differences do not reach statistical significance. This phenomenon is thought to be due to an increase in the water content of the breast during the second half of the menstrual cycle, with ADC values reaching a peak a few days before the onset of menstruation. The reduced ADC value in week 2 of the menstrual cycle is thought to correlate with reduced water content in the breast during this time (53,54). It has been found that there is an increased rate of false-positive findings at contrast-enhanced breast MR imaging during weeks 1 and 4 of the menstrual cycle (54). Therefore, it is recommended that contrast-enhanced breast MR imaging be performed during week 2 of the cycle. In contrast, owing to the lower ADC value of normal breast parenchyma at this time, the difference in signal contrast and ADC value between the normal breast and breast tumor may be smaller in week 2 of the cycle; therefore, diffusion-weighted imaging of the breast may not be appropriate in week 2. Figure 8 shows changes in signal intensity and ADC value during the menstrual cycle.

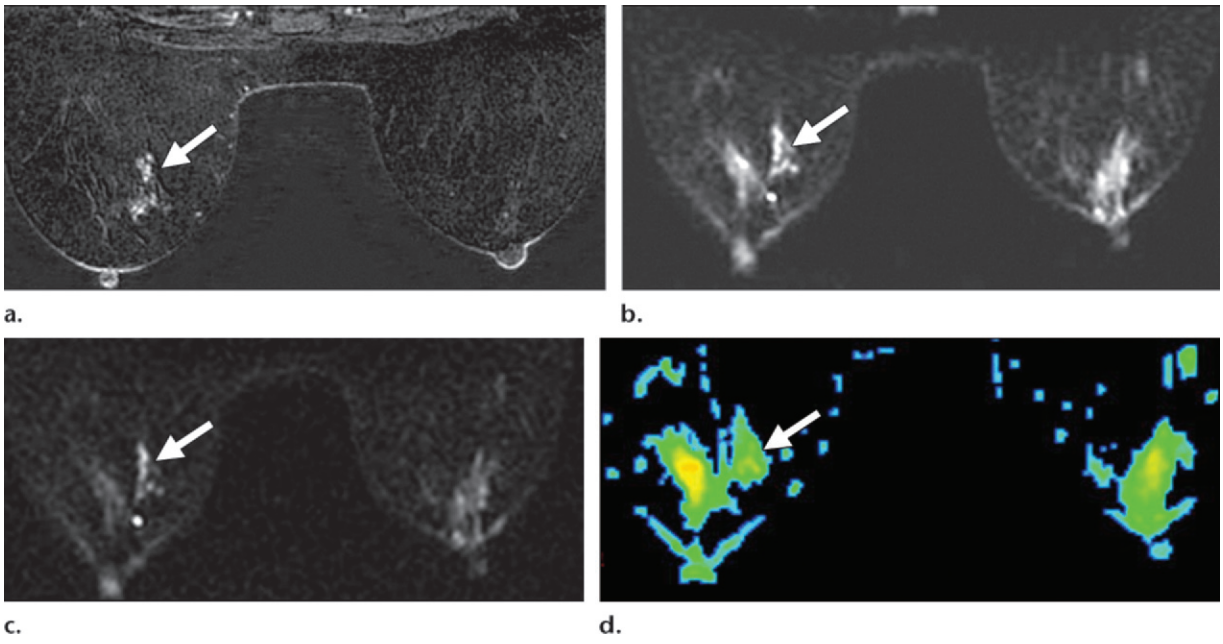

Figure 9. DCIS in the left breast. **(a)** Contrast-enhanced T1-weighted MR image (VIBRANT, TR/TE = 6.5/3.1, flip angle = 12°, bandwidth = ±41.7 kHz, FOV = 360 mm, matrix = 360 × 360, section thickness = 0.9 mm, no intersection gap, SpecIR with ASSET) shows segmental enhancement in the left breast (arrow), a finding that is compatible with DCIS. **(b)** On a diffusion-weighted image obtained at b = 1000 sec/mm^2 (spin-echo echoplanar imaging, TR/TE = 9800/77.6, bandwidth = ±250 kHz, FOV aspect ratio = 0.8 [340 × 272], matrix = 160 × 192, section thickness = 5 mm, no intersection gap, SSRF prepulse without ASSET), the signal intensities of the DCIS (arrow) and normal breast parenchyma are almost equivalent. **(c)** On a diffusion-weighted image obtained at b = 1500 sec/mm^2 (TR/TE = 9800/85.3), the difference between the signal intensity of the DCIS (arrow) and that of normal breast parenchyma is more evident than in **b**. **(d)** On an ADC map obtained at b = 1500 sec/mm^2, the difference between the color of the DCIS (arrow) and that of the surrounding normal breast parenchyma is quite subtle. The ADC value of the DCIS is 1.12 × 10^{-3} mm^2/sec, and that of normal breast parenchyma is 1.48 × 10^{-3} mm^2/sec.

The signal of breast parenchyma is usually suppressed when diffusion-weighted images are acquired at high b values (1000–1500 sec/mm^2). Occasionally, however, dense breast parenchyma will remain hyperintense on high-b-value images (b = 1000 sec/mm^2), potentially masking the signal of malignant tumors (Fig 9). In such cases, an ADC map may be useful for distinguishing between normal breast parenchyma and malignant tumor. However, the detection of DCIS may be difficult on ADC maps alone.

Breast Cancer.—Because of their higher cellularity, the majority of invasive ductal carcinomas (IDCs) demonstrate higher signal intensity and lower ADC values than do benign tumors and normal breast parenchyma on diffusion-weighted images. In addition, there is occasionally central hypointensity in IDCs, which is thought to represent necrosis or fibrosis. This appearance usually corresponds to the appearance on contrast-enhanced T1-weighted MR images. High-resolution diffusion-weighted imaging can display the morphologic features of the tumor, which may be helpful for interpretation (Fig 10). When calculating ADC values, one should avoid including the central necrosis or hemorrhage; otherwise, the resulting ADC value will not reliably reflect the physiologic environment of the tumor (Fig 11).

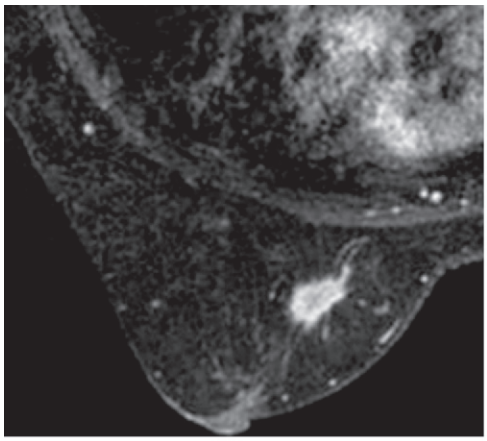

a.

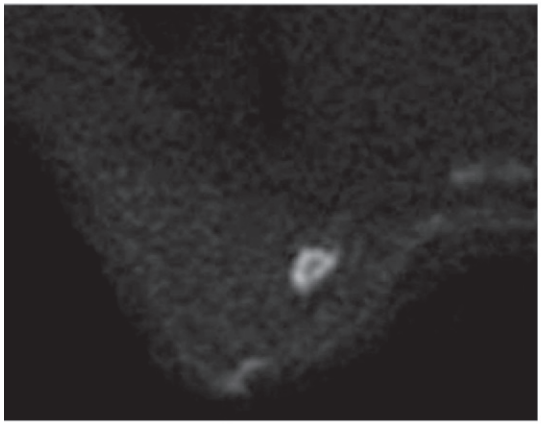

b.

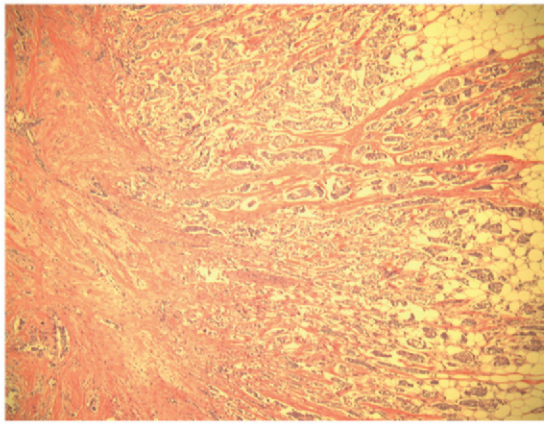

c.

Figure 10. IDC. **(a)** Contrast-enhanced T1-weighted MR image (VIBRANT, TR/TE = 6.5/3.1, flip angle = 12°, bandwidth = ±41.7 kHz, FOV = 360 mm, matrix = 350 × 350, section thickness = 0.9 mm, no intersection gap, SpecIR with ASSET) shows a spiculated mass with peripheral enhancement. **(b)** On a diffusion-weighted image obtained at b = 1500 sec/mm^2 (spin-echo echoplanar imaging, TR/TE = 7800/88.4, bandwidth = ±250 kHz, FOV = 340 mm, matrix = 160 × 192, section thickness = 5 mm, no intersection gap, SSRF prepulse with ASSET), the mass has high signal intensity with marginal spiculation and a central hypointense area. **(c)** Photomicrograph (original magnification, ×200; hematoxylin-eosin stain) shows IDC with central fibrotic change.

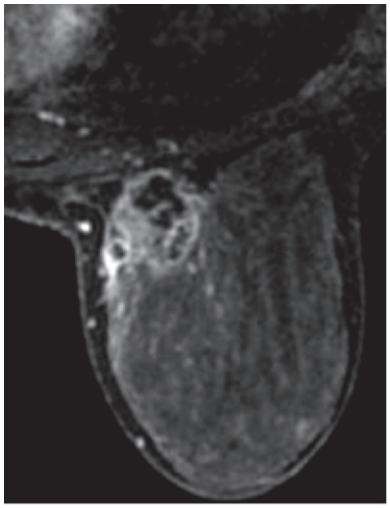

a.

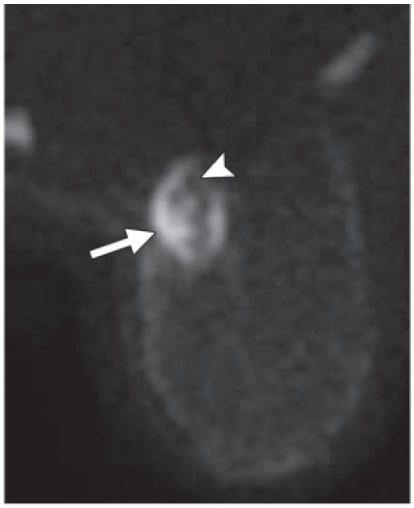

b.

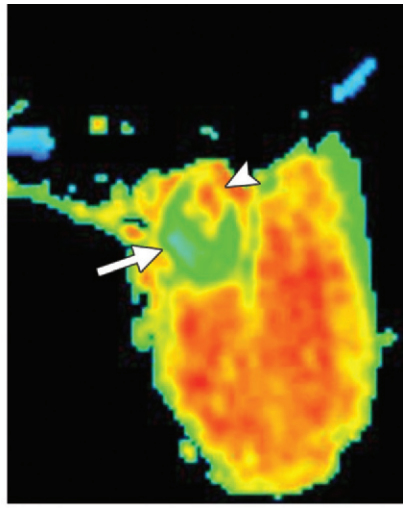

c.

Figure 11. IDC with central necrosis. **(a)** Contrast-enhanced T1-weighted MR image (VIBRANT, TR/TE = 6.5/3.1, flip angle = 12°, bandwidth = ±41.7 kHz, FOV = 360 mm, matrix = 350 × 350, section thickness = 0.9 mm, no intersection gap, SpecIR with ASSET) shows a mass containing an unenhanced area that represents necrosis or degeneration. **(b)** Diffusion-weighted image obtained at b = 1500 sec/mm^2 (spin-echo echoplanar imaging, TR/TE = 7800/88.4, bandwidth = ±250 kHz, FOV = 340 mm, matrix = 160 × 192, section thickness = 5 mm, no intersection gap, SSRF prepulse with ASSET) shows the mass with peripheral high signal intensity (arrow) and central low signal intensity (arrowhead). **(c)** On an ADC map, the ADC value of the high-signal-intensity area (arrow) is 0.89 × 10^{-3} mm^2/sec, and that of the low-signal-intensity area (arrowhead) is 1.81 × 10^{-3} mm^2/sec (cf **b**). The ADC value of a region of interest that encompassed both areas was 1.52 × 10^{-3} mm^2/sec, a finding that indicated a benign tumor.

Figure 12. DCIS and fibrocystic disease. **(a)** Contrast-enhanced T1-weighted MR image (VIBRANT, TR/TE = 7.1/3.4, flip angle = 12°, bandwidth = ±41.7 kHz, FOV = 360 mm, matrix = 400 × 400, section thickness = 0.9 mm, no intersection gap, SpecIR with ASSET) shows bilateral segmental enhancement representing DCIS in the left breast (arrows) and fibrocystic disease in the right breast (arrowheads). **(b)** Diffusion-weighted image obtained at b = 1000 sec/mm^2 (spin-echo echoplanar imaging, TR/TE = 9800/77.6, bandwidth = ±250 kHz, FOV aspect ratio = 0.8 [340 × 272], matrix = 160 × 192, section thickness = 5 mm, no intersection gap, SSRF prepulse without ASSET) shows corresponding hyperintense lesions. Arrows indicate DCIS, arrowheads indicate fibrocystic disease. **(c)** On a diffusion-weighted image obtained at b = 1500 sec/mm^2 (TR/TE = 9800/85.3), the fibrocystic disease (arrowheads) shows a loss in signal intensity (ADC value of 1.01 × 10^{-3} mm^2/sec), whereas the DCIS (arrows) shows an increase in signal intensity (ADC value of 1.17 × 10^{-3} mm^2/sec).

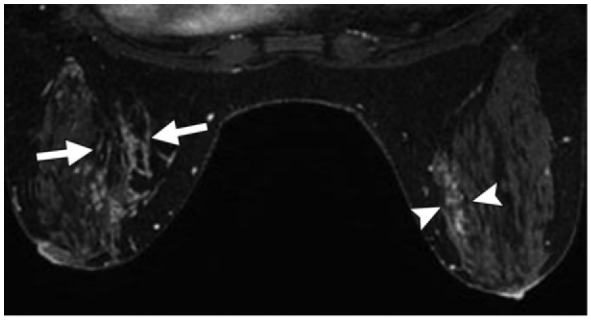

a.

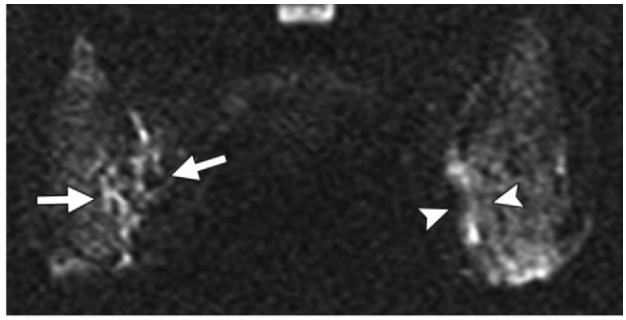

b.

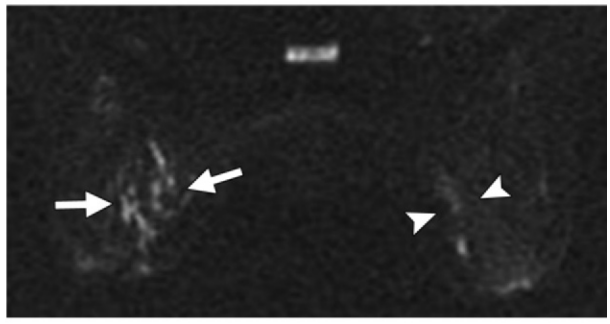

c.

The interpretation of DCIS at diffusion-weighted imaging remains controversial. Mass-forming DCIS will manifest with high signal intensity at diffusion-weighted imaging due to its relatively high cellularity. However, the signal intensity of DCIS with low cellularity (eg, low-grade DCIS) may be ambiguous, especially at higher b values, due to signal decay resulting from the use of higher diffusion gradients. Consequently, most of the false-negative cases reported at diffusion-weighted imaging represent DCIS (5,27,30,37). Therefore, some of the previous reports of ADC values at breast MR imaging omit DCIS cases from their analysis on the assumption that the ADC value of DCIS may not be reliable due to the sparse distribution of cells and the possibility of interspersed normal breast parenchyma. Another problem when assessing DCIS at diffusion-weighted imaging is differentiating between DCIS and fibrocystic disease. On diffusion-weighted images obtained at a high b value, the signal intensity of DCIS remains unchanged while the surrounding fibrocystic disease demonstrates loss of signal intensity. Consequently, the use of higher b values may help distinguish between fibrocystic disease and DCIS. Figure 12 illustrates a case of DCIS and fibrocystic disease.

Invasive lobular carcinoma presents another diagnostic challenge at MR imaging, and its size may be underestimated at diffusion-weighted

Figure 13. Invasive lobular carcinoma. **(a)** Contrast-enhanced T1-weighted MR image (VIBRANT, TR/TE = 7.1/3.4, flip angle = 12°, bandwidth = ±41.7 kHz, FOV = 360 mm, matrix = 400 × 400, section thickness = 0.9 mm, no intersection gap, SpecIR with ASSET) shows an irregular enhanced lesion (arrows) in the upper outer quadrant of the right breast. **(b)** On a diffusion-weighted image obtained at b = 1500 sec/mm^2 (spin-echo echoplanar imaging, TR/TE = 9800/85.3, bandwidth = ±250 kHz, FOV aspect ratio = 0.7 [340 × 238], matrix = 160 × 224, section thickness = 5 mm, no intersection gap, SSRF prepulse without ASSET), the lesion (arrows) has high signal intensity with indistinct margins. **(c)** Photomicrograph (original magnification, ×200; hematoxylin-eosin stain) shows widely distributed interlacing tumor foci in the stromal tissue.

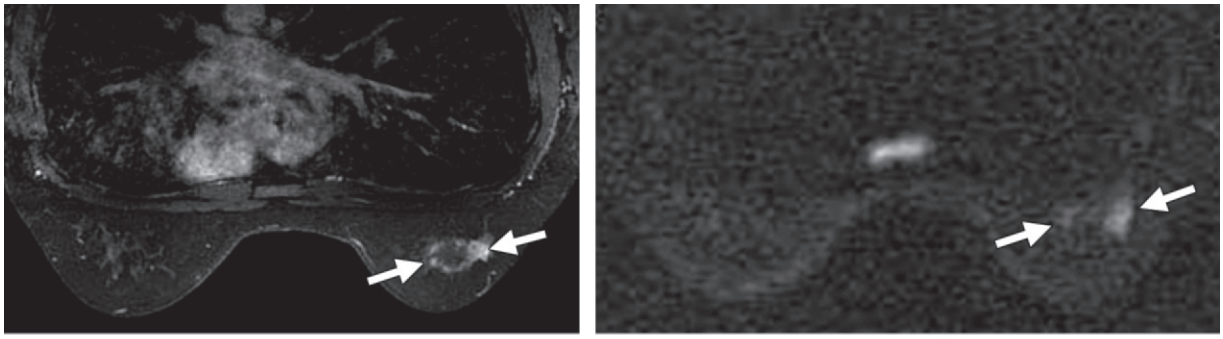

a. b.

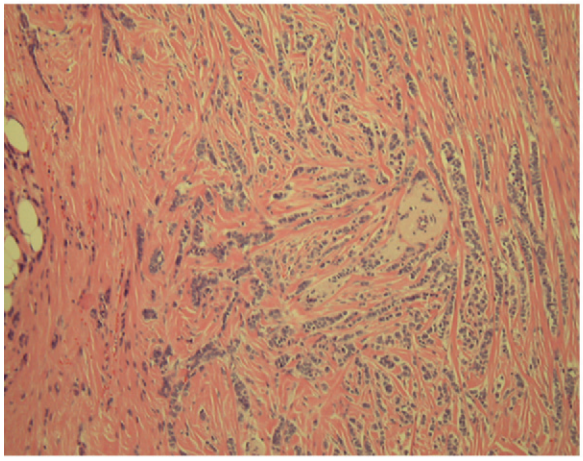

c.

imaging. This inaccuracy may be due to the distribution of infiltrating cells, which lack cohesion, resulting in single lines of low cellularity that can be difficult to detect on low-spatial-resolution images (38). Figure 13 shows an invasive lobular carcinoma. The high-signal-intensity lesion seen at diffusion-weighted imaging has a dim margin that is less conspicuous than that of IDC (Fig 13b). The analysis of ADC values can help distinguish between benignity and malignancy in both masslike and nonmasslike lesions. However, the ADC value of nonmasslike lesions is significantly higher than that of masslike lesions, so that the former may be misdiagnosed as benign lesions (50).

Mucinous carcinoma has a specific appearance at diffusion-weighted imaging (10). It contains a mucin lake compartment, so that its signal intensity remains hyperintense on diffusion-weighted images (obtained at a low b value) and hyperintense on T2-weighted images. At a higher b value, the signal intensity of mucinous carcinoma will decrease at diffusion-weighted imaging due to T2 shine-through. The ADC value of mucinous carcinoma is generally higher than that of IDC, although it varies depending on the cellularity and relative volume of the mucin compartment (10). At diffusion-weighted imaging, an internal structure with heterogeneous high signal intensity and nodular architecture, together with a hypointense

Figure 14. Mucinous carcinoma. **(a)** T2-weighted MR image (fast spin-echo imaging, TR/TE = 5000/88.6, bandwidth = ±31.2 kHz, FOV = 200 mm, matrix = 288 × 192, section thickness = 3 mm, intersection gap = 1 mm, chemical shift saturation) shows a mass with homogeneous high signal intensity and clear margins. A hypointense septumlike structure is seen within the tumor. **(b)** On a diffusion-weighted image obtained at b = 1500 sec/mm^2 (spin-echo echoplanar imaging, TR/TE = 9800/85.3, bandwidth = ±250 kHz, FOV aspect ratio = 0.7 [340 × 238], matrix = 160 × 192, section thickness = 5 mm, no intersection gap, SSRF prepulse without ASSET), the mass (arrows) has low signal intensity and cannot easily be detected. **(c)** On an ADC map, the mass has a homogeneous high ADC value (2.61 × 10^{-3} mm^2/sec).

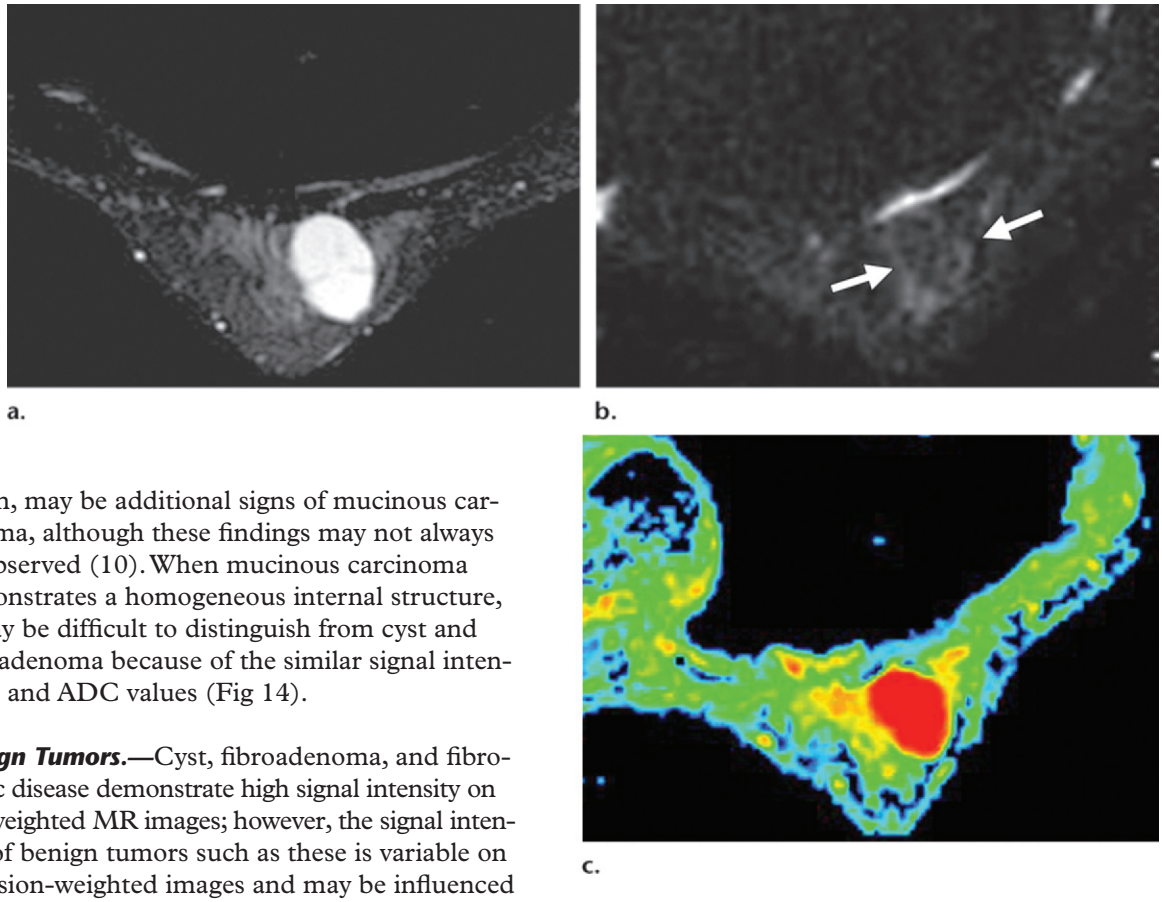

a. b. c.

lesion, may be additional signs of mucinous carcinoma, although these findings may not always be observed (10). When mucinous carcinoma demonstrates a homogeneous internal structure, it may be difficult to distinguish from cyst and fibroadenoma because of the similar signal intensities and ADC values (Fig 14).

Benign Tumors.—Cyst, fibroadenoma, and fibrocystic disease demonstrate high signal intensity on T2-weighted MR images; however, the signal intensity of benign tumors such as these is variable on diffusion-weighted images and may be influenced by b value much more than the signal intensity of malignant tumors because of T2 shine-through. These benign tumors may display high signal intensity on diffusion-weighted images obtained at lower b values; on diffusion-weighted images obtained at higher b values, these tumors become isointense and may not be identified (27,30,37,50,55). Table E2 (online) shows the ADC values of benign tumors as reported in previous studies.

Intraductal papilloma is one of the benign breast diseases that can be misdiagnosed as malignancy due to a low ADC value (Fig 15) (5,37). Its diagnosis will remain problematic even with the combined use of ADC value, signal intensity, and morphologic features.

The majority of fibroadenomas have intermediate to low signal intensity relative to IDC at higher b values, and may have a lower signal intensity than that of the surrounding breast parenchyma due to myxomatous change (Figs 16, 17). The ADC value of fibroadenoma is generally higher than that of IDC. In large fibroadenomas, a low-signal-intensity septum may be observed on diffusion-weighted images. Phyllodes tumor

Figure 15. Intraductal papilloma. **(a)** Contrast-enhanced T1-weighted MR image (VIBRANT, TR/TE = 6.5/3.1, flip angle = 12°, bandwidth = ±41.7 kHz, FOV = 360 mm, matrix = 350 × 350, section thickness = 0.9 mm, no intersection gap, SpecIR with ASSET) shows a mass with strong contrast enhancement (arrows). Bilateral areas of diffuse nodular enhancement are observed in the breasts. **(b)** Diffusion-weighted image obtained at b = 1500 sec/mm^2 (spin-echo echoplanar imaging, TR/TE = 7800/88.4, bandwidth = ±250 kHz, FOV = 340 mm, matrix = 160 × 192, section thickness = 5 mm, no intersection gap, SSRF prepulse with ASSET) shows the mass with high signal intensity (arrows). Diffuse hyperintense lesions are also observed. The mass had an ADC value of 0.83 × 10^{-3} mm^2/sec.

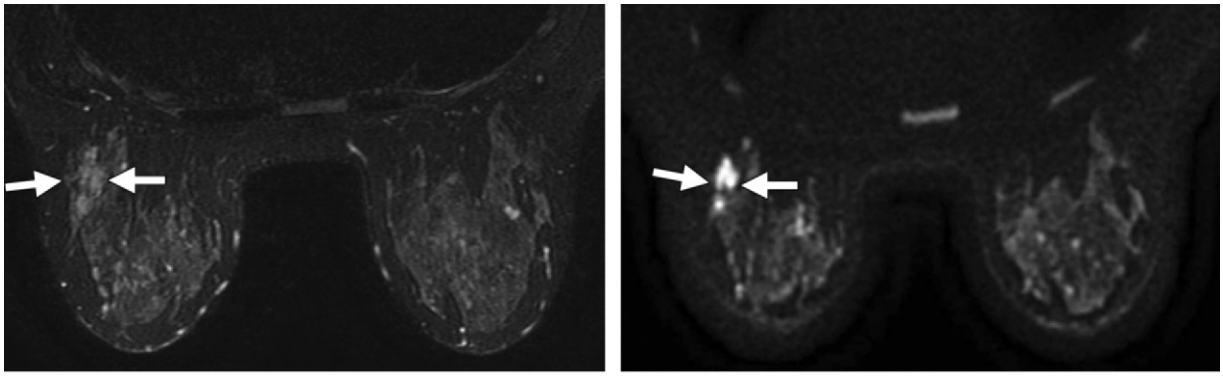

a. b.

Figure 16. Fibroadenoma with myxomatous change. **(a)** T2-weighted MR image (fast spin-echo imaging, TR/TE = 5000/88.6, bandwidth = ±31.2 kHz, FOV = 200 mm, matrix = 288 × 192, section thickness = 3 mm, intersection gap = 1 mm, chemical shift saturation) shows a lobulated mass with high signal intensity and smooth margins. **(b)** On a diffusion-weighted image obtained at b = 1500 sec/mm^2 (spin-echo echoplanar imaging, TR/TE = 9800/85.3, bandwidth = ±250 kHz, FOV aspect ratio = 0.7 [340 × 238], matrix = 160 × 192, section thickness = 5 mm, no intersection gap, SSRF prepulse without ASSET), the signal intensity of the mass (arrows) is close to the noise level. **(c)** ADC map shows the mass with an ADC value of 1.82 × 10^{-3} mm^2/sec.

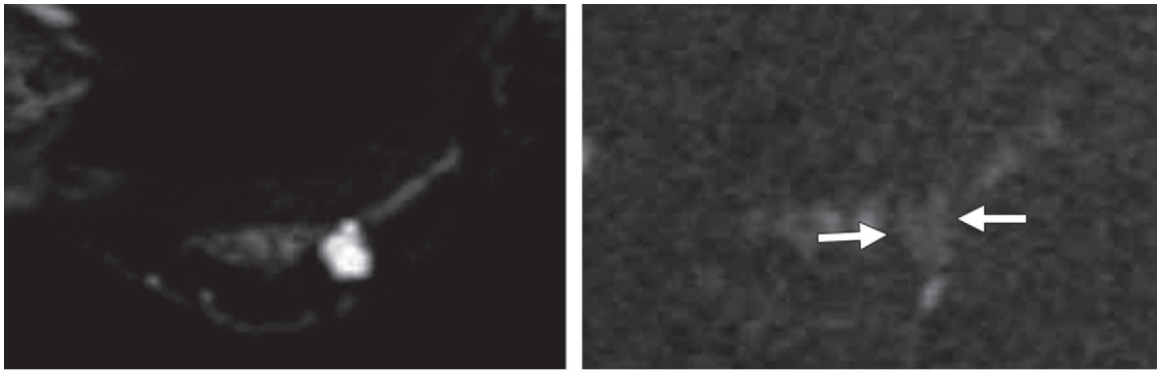

a. b.

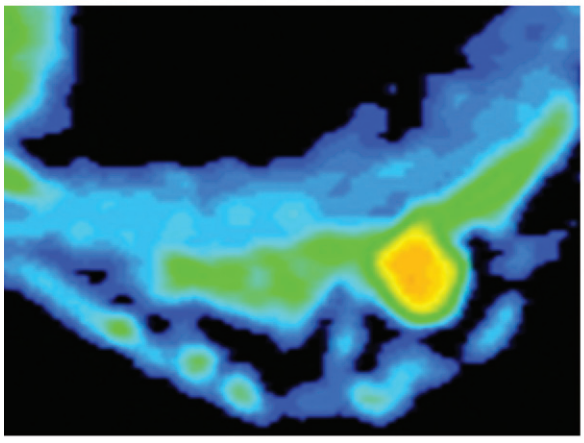

c.

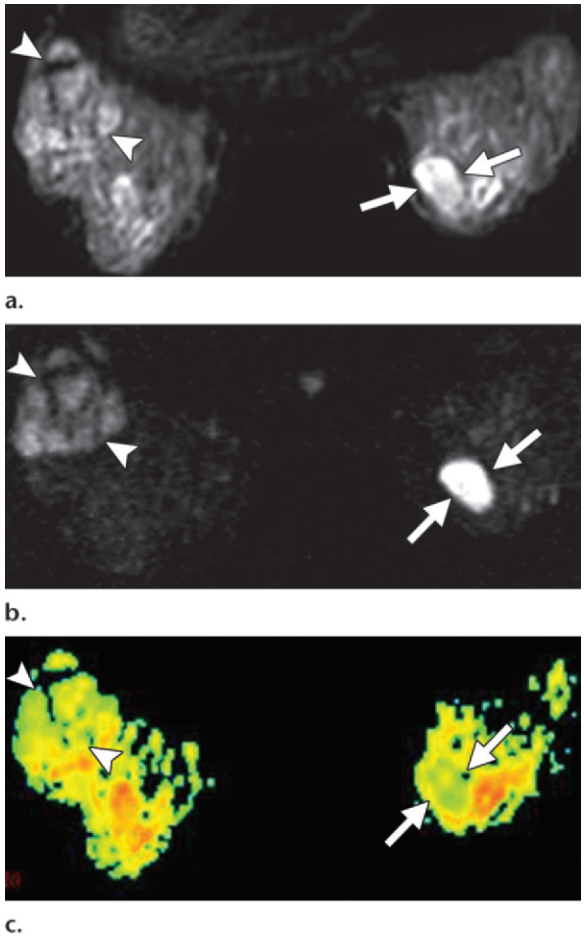

Figure 17. Bilateral multiple fibroadenoma in the breasts. **(a)** Diffusion-weighted image obtained at b = 0 sec/mm^2 shows a hyperintense mass in the left breast (arrowheads) and a mass with even higher signal intensity in the right breast (arrows). Both masses have smooth margins. Diffusion-weighted imaging with a b value of 0 sec/mm^2 is equivalent to fat-saturated T2-weighted imaging. **(b)** On a diffusion-weighted image obtained at b = 1500 sec/mm^2 (spin-echo echoplanar imaging, TR/TE = 9500/88.9, bandwidth = ±250 kHz, FOV aspect ratio = 0.8 [340 × 272], matrix = 160 × 224, section thickness = 6 mm, no intersection gap, SSRF prepulse without ASSET), the mass in the left breast (arrowheads) is slightly hyperintense and contains hypointense septumlike structures, findings that are consistent with those seen in **a**. The mass in the right breast (arrows) demonstrates high signal intensity. **(c)** On an ADC map, the left-sided mass (arrowheads) has an ADC value of 1.65 × 10^{-3} mm^2/sec, and the right-sided mass (arrows) has an ADC value of 1.52 × 10^{-3} mm^2/sec.

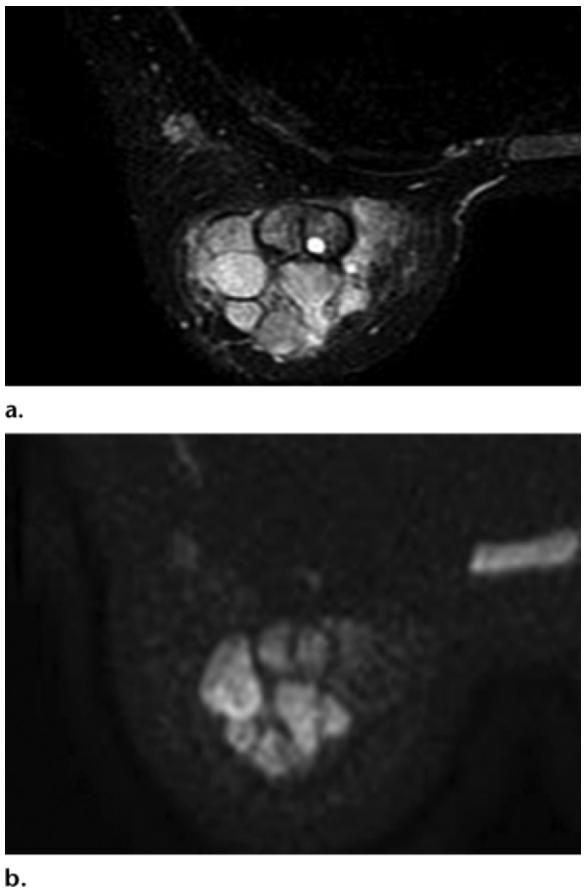

Figure 18. Benign phyllodes tumor. **(a)** T2-weighted MR image (fast spin-echo imaging, TR/TE = 5000/88.6, bandwidth = ±31.2 kHz, FOV = 200 mm, matrix = 288 × 192, section thickness = 3 mm, intersection gap = 1 mm, chemical shift saturation) shows a lobulated mass containing hypointense septumlike structures. **(b)** Diffusion-weighted image (spin-echo echoplanar imaging, TR/TE = 8200/75.3, bandwidth = ±250 kHz, FOV = 340 × 340, matrix = 160 × 192, section thickness = 5 mm, no intersection gap, SSRF prepulse with ASSET) shows similar findings. The ADC value of the mass was 1.51 × 10^{-3} mm^2/sec.

may manifest with a lobulated shape and a hypointense septum, appearing similar to fibroadenoma (Fig 18).

The appearance of fibrocystic disease at diffusion-weighted imaging is variable, with diffuse, bilateral nodular, or segmental high signal intensity being typical. In addition, in the majority of cases, the signal intensity of fibrocystic disease decreases as b value increases (Fig 19); thus, imaging at a higher b value may be useful in differentiating between DCIS and fibrocystic disease. In some cases, however, fibrocystic disease remains hyper-

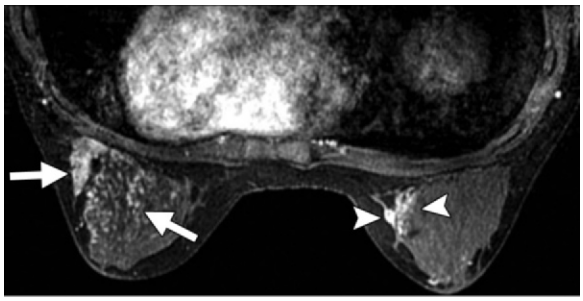

a.

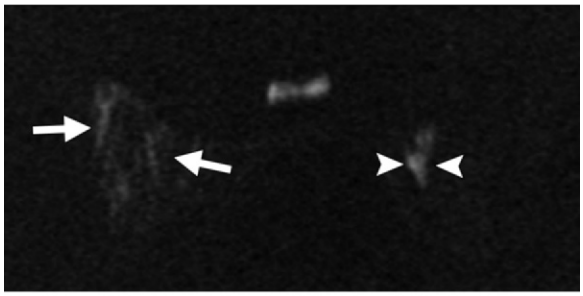

b.

Figure 19. Bilateral fibrocystic disease in the breasts. **(a)** Contrast-enhanced T1-weighted MR image (VIBRANT, TR/TE = 6.5/3.1, flip angle = 12°, bandwidth = ±41.7 kHz, FOV = 360 mm, matrix = 350 × 350, section thickness = 0.9 mm, no intersection gap, SpecIR with ASSET) shows segmental enhancement in the left (arrows) and right (arrowheads) breasts, findings that mimic the appearance of DCIS. **(b)** Diffusion-weighted image obtained at b = 1500 sec/mm^2 (spin-echo echoplanar imaging, TR/TE = 9800/85.3, bandwidth = ±250 kHz, FOV aspect ratio = 0.7 [340 × 238], matrix = 160 × 192, section thickness = 5 mm, no intersection gap, SSRF prepulse without ASSET) reveals a lesion with segmental hyperintensity in the right breast (arrowheads) and a less conspicuous lesion, which is only slightly hyperintense (arrows), in the left breast. The ADC value of the right-sided lesion was 1.0 × 10^{-3} mm^2/sec, and that of the left-sided lesion was 0.9 × 10^{-3} mm^2/sec. Both lesions could be misdiagnosed as malignant.

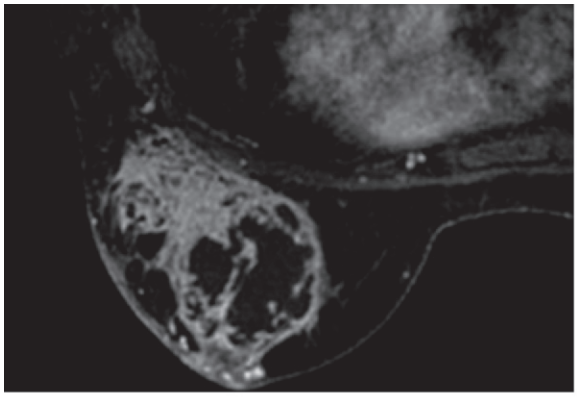

a.

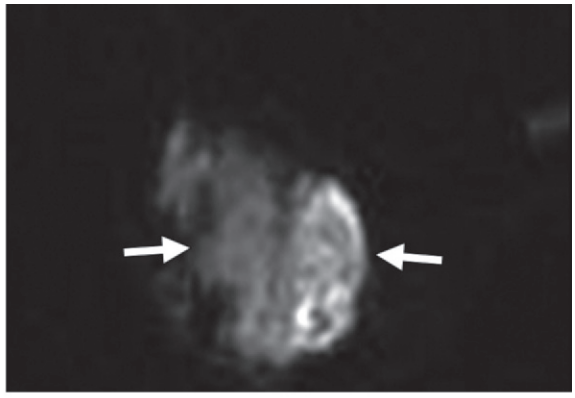

b.

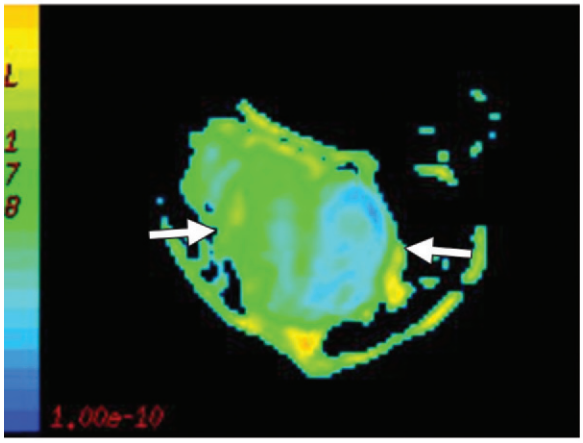

c.

Figure 20. Mastitis. **(a)** Contrast-enhanced T1-weighted MR image (VIBRANT, TR/TE = 6.5/3.1, flip angle = 12°, bandwidth = ±41.7 kHz, FOV = 320 mm, matrix = 350 × 350, section thickness = 0.9 mm, no intersection gap, SpecIR with ASSET) shows a mass containing unenhanced areas surrounded by areas of heterogeneous contrast enhancement. **(b)** On a diffusion-weighted image obtained at b = 1500 sec/mm^2 (spin-echo echoplanar imaging, TR/TE = 9800/85.3, bandwidth = ±250 kHz, FOV = 340 × 272, matrix = 160 × 192, section thickness = 5 mm, no intersection gap, SSRF prepulse without ASSET), the mass demonstrates high signal intensity (arrows). The surrounding area has relatively lower signal intensity. **(c)** On an ADC map, the mass (arrows), which proved to be a fluid collection, has an ADC value of 0.65 × 10^{-3} mm^2/sec.

intense on diffusion-weighted images obtained at a high b value (>1500 sec/mm^2), so that segmental distribution of fibrocystic disease may be confused with DCIS. ADC value may not help distinguish between DCIS and fibrocystic disease.

Abscess and mastitis both have low ADC values similar to those of malignant tumors (Fig 20). The area of low ADC value within an abscess usually has high signal intensity on T2-weighted images,

which indicates the high water content and high viscosity of the abscess. In clinical practice, physical examination findings should be considered when assessing these entities, thereby simplifying the radiologic diagnosis.

The signal intensity of cysts remains high at *b* values of 1000 sec/mm² or lower, which are commonly used in breast MR imaging. A simple cyst shows greatly reduced signal intensity on an image obtained at a *b* value of 1500 sec/mm² compared with an image obtained at a *b* value of 1000 sec/mm² with the same window setting (Fig 21). However, a cyst with condensed or proteinaceous content sometimes has high signal intensity, even at higher *b* values. Hemorrhage has variable signal intensity and ADC values on diffusion-weighted images (Fig 22). Similarly, hematomas containing intracellular components (intracellular oxyhemoglobin, deoxyhemoglobin, or methemoglobin) show significantly reduced diffusion compared with hematomas containing lysed red blood cells (extracellular methemoglobin) (56,57). Some hematomas have high signal intensity on precontrast T1-weighted images; therefore, T1-weighted images should be evaluated together with diffusion-weighted images to avoid misdiagnosis.

Teaching Point

Influence of Contrast Agent at Diffusion-weighted Imaging

The effect of contrast agent at diffusion-weighted imaging has been discussed in several studies (58–62). The majority of studies show a tendency for the ADC value to decrease after contrast enhancement, although this decrease was not statistically significant in some studies (58–62). Definitive guidelines regarding this issue have yet to be determined. Yuen et al (62) showed a significant reduction in the ADC value of breast tumors on postcontrast diffusion-weighted images as opposed to precontrast diffusion-weighted images. This finding suggests a correlation between the degree of contrast material uptake and decrease in ADC value. However, another study failed to demonstrate any significant difference between ADC values calculated from precontrast diffusion-weighted images and those calculated from postcontrast diffusion-weighted images (7). Possible reasons for the discrepancy between the results of these studies include the different acquisition parameters used, including different time delays between contrast material injection and diffusion-weighted image acquisition. The most

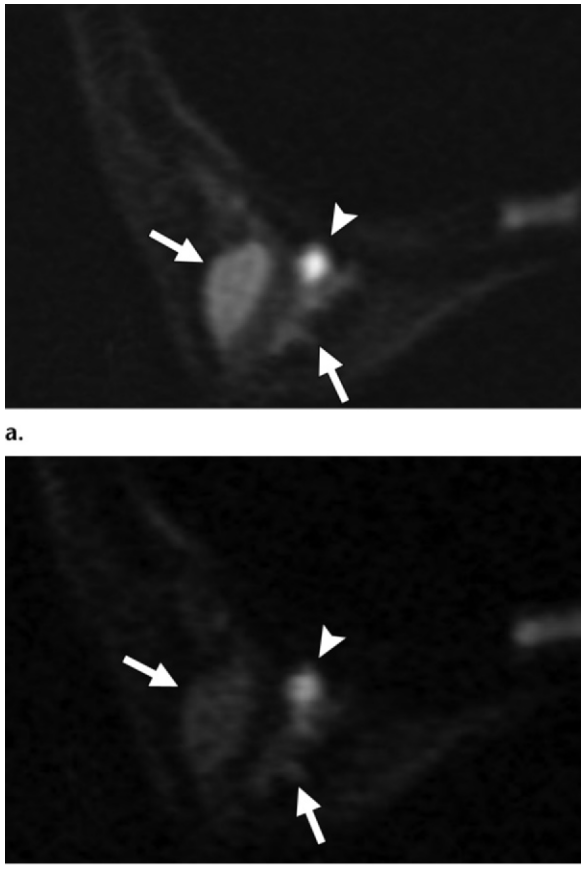

Figure 21. Multiple cysts. **(a)** Diffusion-weighted image obtained at *b* = 1000 sec/mm² (spin-echo echoplanar imaging, TR/TE = 9800/77.6, bandwidth = ±250 kHz, FOV aspect ratio = 0.8 [340 × 272], matrix = 160 × 192, section thickness = 5 mm, no intersection gap, SSRF prepulse without ASSET) shows two hypointense cysts (arrows) and one hyperintense cyst (arrowhead). **(b)** On a diffusion-weighted image obtained at *b* = 1500 sec/mm² (TR/TE = 9800/85.3), the cyst that was hyperintense in **a** retains much of its high signal intensity (arrowhead), whereas the other two cysts demonstrate marked loss of signal intensity (arrows).

widely accepted theory regarding the mechanism of decrease in ADC value after the injection of gadolinium-based contrast material is the change of local magnetic susceptibilities or T2 shortening effect following contrast material uptake (63). The ADC value after contrast enhancement may not be consistent depending on the diffusion-weighted imaging parameters; therefore, it is recommended that diffusion-weighted images be acquired before contrast enhancement to avoid inconsistency between studies. Figure 23 illustrates changes in the ADC value of various pathologic conditions of the breast 10 minutes after the injection of gadopentetate dimeglumine (0.1 mmol/kg).

Teaching Point

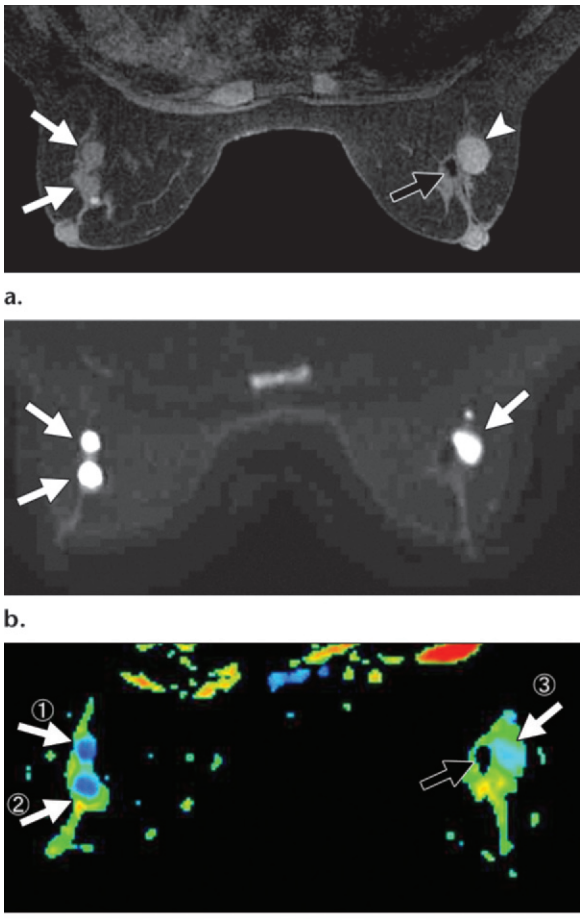

Figure 22. Hemorrhage. **(a)** Unenhanced T1-weighted MR image (VIBRANT, TR/TE = 6.5/3.1, flip angle = 12°, bandwidth = ±41.7 kHz, FOV = 320 mm, matrix = 350 × 350, section thickness = 0.9 mm, no intersection gap, SpecIR with ASSET) shows bilateral cysts in the breasts. The cysts in the left breast (white arrows) demonstrate intermediate signal intensity. A cyst in the right breast (arrowhead) is slightly hyperintense relative to a small unenhanced lesion (black arrow). **(b)** On a diffusion-weighted image obtained at b = 1500 sec/mm^2 (spin-echo echoplanar imaging, TR/TE = 7800/88.4, bandwidth = ±250 kHz, FOV = 340 mm, matrix = 160 × 192, section thickness = 5 mm, no intersection gap, SSRF prepulse with ASSET), the cysts (arrows) show high signal intensity. **(c)** On an ADC map, all three cysts (white arrows) have low ADC values (*1* = 0.31 × 10^{-3} mm^2/sec, *2* = 0.35 × 10^{-3} mm^2/sec, *3* = 0.64 × 10^{-3} mm^2/sec). The hypointense lesion (black arrow) shows noise, a finding that was thought to result from hemosiderin deposition.

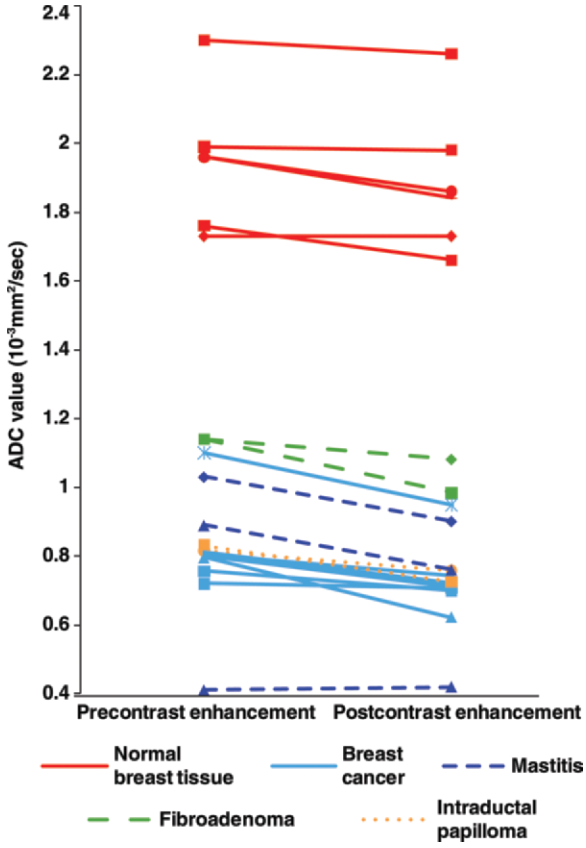

Figure 23. Graph illustrates changes in the ADC value of various pathologic conditions of the breast 10 minutes after the injection of gadopentetate dimeglumine.

Clinical Implementation of Diffusion-weighted Breast Imaging

The most significant advantage of diffusion-weighted imaging over contrast-enhanced MR imaging is its high sensitivity in the detection of breast cancer without contrast material injection. The desire to limit exposure to contrast agents is increasing because of a growing awareness of nephrogenic systemic fibrosis; however, as discussed earlier, diffusion-weighted imaging findings cannot be assessed in isolation from findings obtained with other MR imaging sequences (eg, T2-weighted imaging) because diffusion-weighted imaging has a low specificity for breast cancer and a low sensitivity for the detection of DCIS. However, the assessment of all these findings in combination indicates that diffusion-weighted imaging may have potential as an adjunct to conventional contrast-enhanced breast MR imaging. Further studies assessing the diagnostic utility of non-contrast-enhanced breast MR imaging (eg, diffusion-weighted imaging, T2-weighted and fat-suppressed T1-weighted imaging, ADC map) are required before patients are routinely examined without the use of gadolinium-based contrast material.

In cases of fibrocystic disease with multiple bilateral areas of enhancement in the breasts, diffusion-weighted imaging occasionally depicts small cancers (Fig 12). Diffusion-weighted images obtained at a higher *b* value show high signal contrast between a malignant lesion and normal breast parenchyma, thereby allowing visualization of the lesion. Diffusion-weighted imaging may prove useful in detecting lesions in this setting or in detecting contralateral breast cancer.

Assessment of Neoadjuvant Chemotherapy with Diffusion-weighted Imaging

Several recent studies have shown the potential of diffusion-weighted imaging in helping predict the effect of neoadjuvant chemotherapy (38,48,64–66). In previous diffusion-weighted imaging studies performed to examine rats with breast cancer and brain tumors, the ADC value increased within 2–4 days after chemotherapy (67,68). In these studies, pathologic specimens obtained in the rats 0–14 days after chemotherapy showed a marked increase in tumor extracellular space, a noticeable increase in pleomorphism, large cells, apoptosis, and peritumoral edema. A decrease in cellularity after neoadjuvant chemotherapy was also documented. Diffusion-weighted imaging is expected to be sensitive to the changes in biologic environment brought about by the cytotoxic effect associated with chemotherapeutic agents. These changes cause an increase in the mobility of water in the damaged tissue, which is reflected in the increase in ADC value. In human breast tissue, an increase in ADC value following successful therapy has been observed in some studies. Furthermore, the ADC value increased earlier than lesion size decreased, and change was detected as early as upon completion of the first cycle of neoadjuvant chemotherapy (65,66). Accordingly, ADC value may provide an earlier biomarker for tumor response than changes in tumor size. Early prediction of the effect of chemotherapy would allow timely optimization of the therapy protocol to ensure the best therapeutic effect.

Another potential clinical application of diffusion-weighted imaging is the evaluation of residual breast cancer following neoadjuvant chemotherapy, since residual disease must be resected because failure to do so may affect patient prognosis. Residual disease has historically been evaluated with dynamic contrast-enhanced imaging; however, false-positive and false-negative findings have been observed (69–74). One previous study documented the same accuracy for diffusion-weighted imaging and contrast-enhanced MR imaging in the detection of residual tumor (38). In this study, diffusion-weighted imaging helped detect residual cancers that contrast-enhanced MR imaging did not help detect (Fig 24) (38). Therefore, diffusion-weighted imaging may increase diagnostic accuracy in the evaluation of chemotherapy effect and the detection of residual disease.

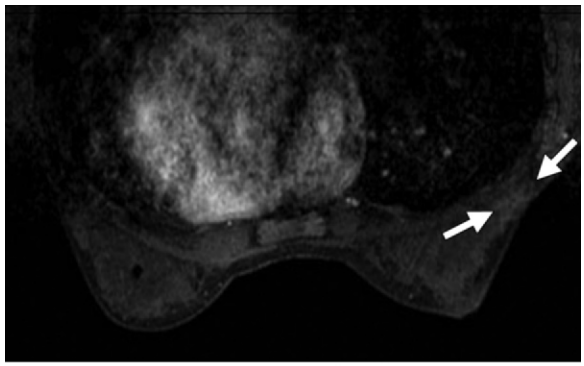

a.

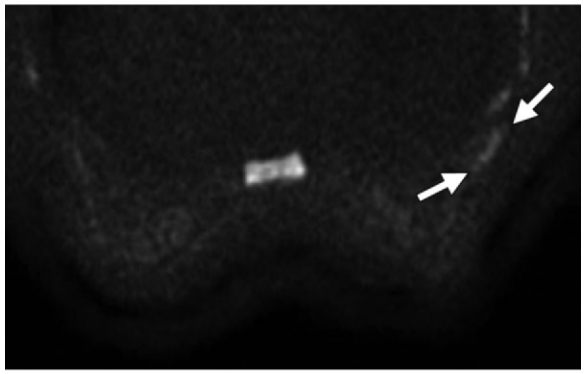

b.

Figure 24. IDC after neoadjuvant chemotherapy. **(a)** Diffusion-weighted image obtained at b = 1500 sec/mm^2 (spin-echo echoplanar imaging, TR/TE = 7800/88.4, bandwidth = ±250 kHz, FOV = 340 mm, matrix = 160 × 192, section thickness = 5 mm, no intersection gap, SSRF prepulse with ASSET) shows a slightly hyperintense focal lesion (arrows) in the location of the original tumor. **(b)** On a contrast-enhanced T1-weighted MR image (VIBRANT, TR/TE = 6.5/3.1, flip angle = 12°, bandwidth = ±41.7 kHz, FOV = 360 mm, matrix = 350 × 350, section thickness = 0.9 mm, no intersection gap, SpecIR with ASSET), the lesion (arrows) shows weak enhancement, a finding that is not likely to indicate residual cancer. Pathologic analysis showed residual IDC.

Diffusion-weighted Imaging at 3.0 T

The majority of published diffusion-weighted breast imaging studies have been conducted at 1.5 T. However, 3.0-T diffusion-weighted imaging with the appropriate acquisition parameters affords a higher SNR per unit time. The inherent increase in SNR can be used to either reduce imaging time or increase spatial resolution. On the

other hand, 3.0-T imaging has several disadvantages. The higher magnetic field strength results in an increase in chemical shift artifact, susceptibility artifact, and B_1 and B_0 inhomogeneity, which can cause image distortion and inhomogeneous fat suppression (75). Nevertheless, the increased susceptibility artifact and nonuniformity in the magnetic field can be minimized with parallel imaging techniques. Likewise, additional shimming and manual optimization of the center frequency are essential to reduce the influence of the aforementioned artifacts. There have been several published diffusion-weighted breast imaging studies undertaken at 3.0 T (76,77). Matsuoka et al (76) demonstrated a greater visibility of tumors less than 10 mm at 3.0 T than at 1.5 T, but no difference in visibility for tumors greater than 10 mm. This finding was attributed to the increased SNR afforded by the increase in magnetic field strength. The greater SNR at 3.0 T than at 1.5 T will likely also prove beneficial when a higher *b* value is used, especially for the evaluation of DCIS. These results have been confirmed in another study conducted at 3.0 T (78), in which ADC values were found to be the same at 1.5 T and 3 T, a finding that is consistent with the premise that ADC values are independent of field strength (76).

Drawbacks and Limitations of Diffusion-weighted Imaging

There are some technical drawbacks with diffusion-weighted imaging. Low SNR can compromise a diffusion-weighted image, so that TE must be shortened to avoid unnecessary T2* losses, whereas TR must be long enough to accommodate T1 relaxation. Multiple averages can be used to improve SNR, although, of course, at the expense of longer imaging time. When multiple averages are acquired, it is recommended that the individual images be reconstructed first so as to avoid any phase errors that may arise from patient motion. High *b* values must be avoided because SNR degrades under these conditions and can cause imaging table vibrations due to large diffusion gradient amplitude, resulting in image artifacts.

As B_0 increases, susceptibility artifacts can become more apparent and problematic. Susceptibility changes occur at sharp transitions between different tissue types (eg, bone-tissue or tissue-air interfaces), creating a change in the localized magnetic field that can give rise to image artifacts. Use of a spin-echo–based sequence, high imaging bandwidth, and short TE can reduce the impact from this artifact.

Voluntary patient movement can also be a potential source of image artifact by causing image misregistration, which leads to false ADC values. Such movement can be eliminated by making sure that the patient is lying in a comfortable position, with the required supporting pads and restraints.

One of the limitations of diffusion-weighted imaging is low spatial resolution. Small cancer foci, including DCIS and scattered foci of invasive lobular cancer, may not be depicted at diffusion-weighted imaging. The higher SNR afforded by imagers with higher magnetic field strength can be used to increase the spatial resolution of diffusion-weighted imaging, thereby allowing the detection and characterization of smaller lesions.

Hemorrhage may have high signal intensity and a low ADC value; consequently, it can be misdiagnosed as malignant lesions. Fat-suppressed T1-weighted images need to be interpreted in conjunction with diffusion-weighted images to avoid making this misdiagnosis.

Nonmasslike lesions, including DCIS, fibrocystic disease, and lobular carcinoma, may contain interspersed normal fibroglandular tissue or fat tissue, which can affect the measured ADC value. Fibrocystic disease may mimic DCIS in terms of ADC value and signal intensity owing to the similar disease formation and cellularity of the two conditions. Tozaki and Fukuma (37) reported eight false-negative cases of non-mass-forming DCIS. Thus, it is important to keep in mind the possibility of overlooking DCIS at diffusion-weighted imaging.

Intraductal papilloma can be misdiagnosed as malignancy. A lesion with a low ADC value and a diffuse, segmental bilateral distribution may indicate intraductal papilloma.

Mucinous carcinoma may be misdiagnosed as fibroadenoma or cyst because it has multiple internal architectures. It is essential to detect the compartment with a higher ADC value (suggesting a mucin lake compartment) to help differentiate mucinous carcinoma from fibroadenoma or, conversely, a compartment with a low ADC value (suggesting a solid mass compartment) to help differentiate it from cyst.

For measurement of ADC value, the lesion must first be identified on an ADC map. This is best accomplished by identifying the lesion on diffusion-weighted images and then carefully placing a region of interest over the solid portion of the tumor to ensure that cystic or necrotic portions or normal breast parenchyma are not included in this region. For small lesions that may be difficult to visualize on diffusion-weighted images and an ADC map because of low spatial resolution, it may be necessary to view the T2-weighted imaging results obtained at a higher spatial resolution.

Future Applications of Diffusion-weighted Imaging

The growth of diffusion-weighted breast imaging as a research tool implies that this modality has potential as an adjunct in the radiologic diagnosis of breast cancer (49). However, the standard protocol for diffusion-weighted breast imaging has yet to be agreed upon, and standardization is necessary to address discrepancies among various published studies. In particular, the optimal *b* value has yet to be determined, and the *b* value exerts great influence on signal intensity and determination of the ADC value. In addition, the appropriate use of nonenhanced breast MR imaging, including diffusion-weighted imaging, needs to be determined for patients with allergy or sensitivity to contrast material, asthma, or renal dysfunction. Furthermore, the clinical benefit of adding diffusion-weighted imaging to standard contrast-enhanced MR imaging protocols needs to be determined, along with the potential of diffusion-weighted imaging as a screening tool because of its high sensitivity to malignancy without the use of contrast material. Ei Khouli et al (51) showed an increase in diagnostic accuracy by adding diffusion-weighted imaging to conventional breast MR imaging at 3.0 T. Their results imply that the use of diffusion-weighted imaging may contribute to more accurate diagnosis in the future. If diffusion-weighted breast imaging proves useful in the clinical setting, it promises to improve the accuracy of breast MR imaging.

The technical development of multichannel array coils as well as the optimization of acquisition parameters will improve SNR and spatial resolution, which should translate into greater accuracy in lesion detection and evaluation.

Conclusions

Understanding the additive value of combining diffusion-weighted imaging, T2-weighted MR imaging, and ADC value for the assessment of breast disease will be useful in the interpretation of breast MR images. It is likely that diffusion-weighted breast imaging will be shown to have a supportive role in breast MR imaging.

The parameters of diffusion-weighted imaging need to be standardized to allow comparison of multicenter studies and assessment of the clinical utility of diffusion-weighted imaging findings and ADC values obtained in the breast.

References

1. Koh DM, Collins DJ. Diffusion-weighted MRI in the body: applications and challenges in oncology. AJR Am J Roentgenol 2007;188(6):1622–1635.
2. Englander SA, Uluğ AM, Brem R, Glickson JD, van Zijl PC. Diffusion imaging of human breast. NMR Biomed 1997;10(7):348–352.
3. Kuroki Y, Nasu K, Kuroki S, et al. Diffusion-weighted imaging of breast cancer with the sensitivity encoding technique: analysis of the apparent diffusion coefficient value. Magn Reson Med Sci 2004; 3(2):79–85.
4. Guo Y, Cai YQ, Cai ZL, et al. Differentiation of clinically benign and malignant breast lesions using diffusion-weighted imaging. J Magn Reson Imaging 2002;16(2):172–178.
5. Woodhams R, Matsunaga K, Kan S, et al. ADC mapping of benign and malignant breast tumors. Magn Reson Med Sci 2005;4(1):35–42.
6. Woodhams R, Matsunaga K, Iwabuchi K, et al. Diffusion-weighted imaging of malignant breast tumors: the usefulness of apparent diffusion coefficient (ADC) value and ADC map for the detection of malignant breast tumors and evaluation of cancer extension. J Comput Assist Tomogr 2005;29(5): 644–649.
7. Rubesova E, Grell AS, De Maertelaer V, Metens T, Chao SL, Lemort M. Quantitative diffusion imaging in breast cancer: a clinical prospective study. J Magn Reson Imaging 2006;24(2):319–324.
8. Marini C, Iacconi C, Giannelli M, Cilotti A, Moretti M, Bartolozzi C. Quantitative diffusion-weighted MR imaging in the differential diagnosis of breast lesion. Eur Radiol 2007;17(10):2646–2655.
9. Kuroki Y, Nasu K. Advances in breast MRI: diffusion-weighted imaging of the breast. Breast Cancer 2008;15(3):212–217.
10. Woodhams R, Kakita S, Hata H, et al. Diffusion-weighted imaging of mucinous carcinoma of the breast: evaluation of apparent diffusion coefficient and signal intensity in correlation with histologic findings. AJR Am J Roentgenol 2009;193(1): 260–266.
11. American College of Radiology. BI-RADS atlas. Reston, Va: American College of Radiology, 2003.
12. Gilles R, Guinebretière JM, Lucidarme O, et al. Nonpalpable breast tumors: diagnosis with contrast-enhanced subtraction dynamic MR imaging. Radiology 1994;191(3):625–631.
13. Boetes C, Strijk SP, Holland R, Barentsz JO, Van Der Sluis RF, Ruijs JH. False-negative MR imaging of malignant breast tumors. Eur Radiol 1997;7(8): 1231–1234.
14. Ghai S, Muradali D, Bukhanov K, Kulkarni S. Nonenhancing breast malignancies on MRI: sonographic and pathologic correlation. AJR Am J Roentgenol 2005;185(2):481–487.
15. Delille JP, Slanetz PJ, Yeh ED, Kopans DB, Garrido L. Breast cancer: regional blood flow and blood volume measured with magnetic susceptibility–based MR imaging—initial results. Radiology 2002;223 (2):558–565.
16. Baron P, Dorrius MD, Kappert P, Oudkerk M, Sijens PE. Diffusion-weighted imaging of normal fibroglandular breast tissue: influence of microperfusion and fat suppression technique on the apparent diffusion coefficient. NMR Biomed 2010;23(4): 399–405.
17. Jin G, An N, Jacobs MA, Li K. The role of parallel diffusion-weighted imaging and apparent diffusion coefficient (ADC) map values for evaluating breast lesions: preliminary results. Acad Radiol 2010;17(4): 456–463.

18. Matsuki M, Inada Y, Nakai G, et al. Diffusion-weighted MR imaging of pancreatic carcinoma. Abdom Imaging 2007;32(4):481–483.
19. Mazaheri Y, Shukla-Dave A, Hricak H, et al. Prostate cancer: identification with combined diffusion-weighted MR imaging and 3D ^{1}H MR spectroscopic imaging—correlation with pathologic findings. Radiology 2008;246(2):480–488.
20. Nasu K, Kuroki Y, Nawano S, et al. Hepatic metastases: diffusion-weighted sensitivity-encoding versus SPIO-enhanced MR imaging. Radiology 2006;239(1):122–130.
21. Raya JG, Dietrich O, Reiser MF, Baur-Melnyk A. Methods and applications of diffusion imaging of vertebral bone marrow. J Magn Reson Imaging 2006;24(6):1207–1220.
22. Sugita R, Ito K, Fujita N, Takahashi S. Diffusion-weighted MRI in abdominal oncology: clinical applications. World J Gastroenterol 2010;16(7):832–836.
23. Yoshikawa T, Ohno Y, Kawamitsu H, et al. Abdominal apparent diffusion coefficient measurements: effect of diffusion-weighted image quality and usefulness of anisotropic images. Magn Reson Imaging 2008;26(10):1415–1420.
24. Hatakenaka M, Soeda H, Yabuuchi H, et al. Apparent diffusion coefficients of breast tumors: clinical application. Magn Reson Med Sci 2008;7(1):23–29.
25. Kim SH, Cha ES, Kim HS, et al. Diffusion-weighted imaging of breast cancer: correlation of the apparent diffusion coefficient value with prognostic factors. J Magn Reson Imaging 2009;30(3):615–620.
26. Kinoshita T, Yashiro N, Ihara N, Funatu H, Fukuma E, Narita M. Diffusion-weighted half-Fourier single-shot turbo spin echo imaging in breast tumors: differentiation of invasive ductal carcinoma from fibroadenoma. J Comput Assist Tomogr 2002;26(6):1042–1046.
27. Kuroki-Suzuki S, Kuroki Y, Nasu K, Nawano S, Moriyama N, Okazaki M. Detecting breast cancer with non-contrast MR imaging: combining diffusion-weighted and STIR imaging. Magn Reson Med Sci 2007;6(1):21–27.
28. Park MJ, Cha ES, Kang BJ, Ihn YK, Baik JH. The role of diffusion-weighted imaging and the apparent diffusion coefficient (ADC) values for breast tumors. Korean J Radiol 2007;8(5):390–396.
29. Sinha S, Lucas-Quesada FA, Sinha U, DeBruhl N, Bassett LW. In vivo diffusion-weighted MRI of the breast: potential for lesion characterization. J Magn Reson Imaging 2002;15(6):693–704.
30. Baltzer PA, Benndorf M, Dietzel M, Gajda M, Camara O, Kaiser WA. Sensitivity and specificity of unenhanced MR mammography (DWI combined with T2-weighted TSE imaging, ueMRM) for the differentiation of mass lesions. Eur Radiol 2010;20(5):1101–1110.
31. Wenkel E, Geppert C, Schulz-Wendtland R, et al. Diffusion weighted imaging in breast MRI: comparison of two different pulse sequences. Acad Radiol 2007;14(9):1077–1083.
32. Kazama T, Nasu K, Kuroki Y, Nawano S, Ito H. Comparison of diffusion-weighted images using short inversion time inversion recovery or chemical shift selective pulse as fat suppression in patients with breast cancer. Jpn J Radiol 2009;27(4):163–167.
33. Heidemann RM, Ozsarlak O, Parizel PM, et al. A brief review of parallel magnetic resonance imaging. Eur Radiol 2003;13(10):2323–2337.
34. Pruessmann KP, Weiger M, Scheidegger MB, Boesiger P. SENSE: sensitivity encoding for fast MRI. Magn Reson Med 1999;42(5):952–962.
35. Le Bihan D, Breton E, Lallemand D, Grenier P, Cabanis E, Laval-Jeantet M. MR imaging of intravoxel incoherent motions: application to diffusion and perfusion in neurologic disorders. Radiology 1986;161(2):401–407.
36. Bammer R. Basic principles of diffusion-weighted imaging. Eur J Radiol 2003;45(3):169–184.
37. Tozaki M, Fukuma E. 1H MR spectroscopy and diffusion-weighted imaging of the breast: are they useful tools for characterizing breast lesions before biopsy? AJR Am J Roentgenol 2009;193(3):840–849.
38. Woodhams R, Kakita S, Hata H, et al. Identification of residual breast carcinoma following neoadjuvant chemotherapy: diffusion-weighted imaging—comparison with contrast-enhanced MR imaging and pathologic findings. Radiology 2010;254(2):357–366.
39. Toyoda K, Kitai S, Ida M, Suga S, Aoyagi Y, Fukuda K. Usefulness of high-b-value diffusion-weighted imaging in acute cerebral infarction. Eur Radiol 2007;17(5):1212–1220.
40. Seo HS, Chang KH, Na DG, Kwon BJ, Lee DH. High b-value diffusion (b = 3000 s/mm^2) MR imaging in cerebral gliomas at 3T: visual and quantitative comparisons with b = 1000 s/mm^2. AJNR Am J Neuroradiol 2008;29(3):458–463.
41. Pereira FP, Martins G, Figueiredo E, et al. Assessment of breast lesions with diffusion-weighted MRI: comparing the use of different b values. AJR Am J Roentgenol 2009;193(4):1030–1035.
42. Mulkern RV, Gudbjartsson H, Westin CF, et al. Multi-component apparent diffusion coefficients in human brain. NMR Biomed 1999;12(1):51–62.
43. Yamada I, Aung W, Himeno Y, Nakagawa T, Shibuya H. Diffusion coefficients in abdominal organs and hepatic lesions: evaluation with intravoxel incoherent motion echo-planar MR imaging. Radiology 1999;210(3):617–623.
44. Moore RJ, Issa B, Tokarczuk P, et al. In vivo intravoxel incoherent motion measurements in the human placenta using echo-planar imaging at 0.5 T. Magn Reson Med 2000;43(2):295–302.
45. Yeung DK, Wong SY, Griffith JF, Lau EM. Bone marrow diffusion in osteoporosis: evaluation with quantitative MR diffusion imaging. J Magn Reson Imaging 2004;19(2):222–228.
46. Mulkern RV, Barnes AS, Haker SJ, et al. Biexponential characterization of prostate tissue water diffusion decay curves over an extended b-factor range. Magn Reson Imaging 2006;24(5):563–568.
47. Yoshikawa MI, Ohsumi S, Sugata S, et al. Relation between cancer cellularity and apparent diffusion coefficient values using diffusion-weighted magnetic resonance imaging in breast cancer. Radiat Med 2008;26(4):222–226.
48. Yankeelov TE, Lepage M, Chakravarthy A, et al. Integration of quantitative DCE-MRI and ADC mapping to monitor treatment response in human breast cancer: initial results. Magn Reson Imaging 2007;25(1):1–13.
49. Yabuuchi H, Matsuo Y, Okafuji T, et al. Enhanced mass on contrast-enhanced breast MR imaging: lesion characterization using combination of dynamic contrast-enhanced and diffusion-weighted MR images. J Magn Reson Imaging 2008;28(5):1157–1165.

50. Partridge SC, Mullins CD, Kurland BF, et al. Apparent diffusion coefficient values for discriminating benign and malignant breast MRI lesions: effects of lesion type and size. AJR Am J Roentgenol 2010;194(6):1664–1673.
51. Ei Khouli RH, Jacobs MA, Mezban SD, et al. Diffusion-weighted imaging improves the diagnostic accuracy of conventional 3.0-T breast MR imaging. Radiology 2010;256(1):64–73.
52. Poon CS, Bronskill MJ, Henkelman RM, Boyd NF. Quantitative magnetic resonance imaging parameters and their relationship to mammographic pattern. J Natl Cancer Inst 1992;84(10):777–781.
53. Partridge SC, McKinnon GC, Henry RG, Hylton NM. Menstrual cycle variation of apparent diffusion coefficients measured in the normal breast using MRI. J Magn Reson Imaging 2001;14(4):433–438.
54. Delille JP, Slanetz PJ, Yeh ED, Kopans DB, Garrido L. Physiologic changes in breast magnetic resonance imaging during the menstrual cycle: perfusion imaging, signal enhancement, and influence of the T1 relaxation time of breast tissue. Breast J 2005;11(4):236–241.
55. Stadlbauer A, Bernt R, Gruber S, et al. Diffusion-weighted MR imaging with background body signal suppression (DWIBS) for the diagnosis of malignant and benign breast lesions. Eur Radiol 2009;19(10):2349–2356.
56. Atlas SW, DuBois P, Singer MB, Lu D. Diffusion measurements in intracranial hematomas: implications for MR imaging of acute stroke. AJNR Am J Neuroradiol 2000;21(7):1190–1194.
57. Fischbein NJ, Roberts TP, Dillon WP. Bleed or stroke? diffusion measurements in intracranial hematomas. AJNR Am J Neuroradiol 2000;21(7):1179–1180.
58. Yamada K, Kubota H, Kizu O, et al. Effect of intravenous gadolinium-DTPA on diffusion-weighted images: evaluation of normal brain and infarcts. Stroke 2002;33(7):1799–1802.
59. Chen G, Jespersen SN, Pedersen M, Pang Q, Horsman MR, Stødkilde-Jørgensen H. Intravenous administration of Gd-DTPA prior to DWI does not affect the apparent diffusion constant. Magn Reson Imaging 2005;23(5):685–689.
60. Chiu FY, Jao JC, Chen CY, et al. Effect of intravenous gadolinium-DTPA on diffusion-weighted magnetic resonance images for evaluation of focal hepatic lesions. J Comput Assist Tomogr 2005;29(2):176–180.
61. Firat AK, Sanli B, Karakaş HM, Erdem G. The effect of intravenous gadolinium-DTPA on diffusion-weighted imaging. Neuroradiology 2006;48(7):465–470.
62. Yuen S, Yamada K, Goto M, Nishida K, Takahata A, Nishimura T. Microperfusion-induced elevation of ADC is suppressed after contrast in breast carcinoma. J Magn Reson Imaging 2009;29(5):1080–1084.
63. Ramadan S, Mulkern RV. Comment on ADC reductions in postcontrast breast tumors. J Magn Reson Imaging 2010;31(1):262; author reply 263–264.
64. Manton DJ, Chaturvedi A, Hubbard A, et al. Neoadjuvant chemotherapy in breast cancer: early response prediction with quantitative MR imaging and spectroscopy. Br J Cancer 2006;94(3):427–435.
65. Pickles MD, Gibbs P, Lowry M, Turnbull LW. Diffusion changes precede size reduction in neoadjuvant treatment of breast cancer. Magn Reson Imaging 2006;24(7):843–847.
66. Sharma U, Danishad KK, Seenu V, Jagannathan NR. Longitudinal study of the assessment by MRI and diffusion-weighted imaging of tumor response in patients with locally advanced breast cancer undergoing neoadjuvant chemotherapy. NMR Biomed 2009;22(1):104–113.
67. Galons JP, Altbach MI, Paine-Murrieta GD, Taylor CW, Gillies RJ. Early increases in breast tumor xenograft water mobility in response to paclitaxel therapy detected by non-invasive diffusion magnetic resonance imaging. Neoplasia 1999;1(2):113–117.
68. Lee KC, Moffat BA, Schott AF, et al. Prospective early response imaging biomarker for neoadjuvant breast cancer chemotherapy. Clin Cancer Res 2007;13(2 pt 1):443–450.
69. Esserman L, Kaplan E, Partridge S, et al. MRI phenotype is associated with response to doxorubicin and cyclophosphamide neoadjuvant chemotherapy in stage III breast cancer. Ann Surg Oncol 2001;8(6):549–559.
70. Rieber A, Brambs HJ, Gabelmann A, Heilmann V, Kreienberg R, Kühn T. Breast MRI for monitoring response of primary breast cancer to neo-adjuvant chemotherapy. Eur Radiol 2002;12(7):1711–1719.
71. Berg WA, Gutierrez L, NessAiver MS, et al. Diagnostic accuracy of mammography, clinical examination, US, and MR imaging in preoperative assessment of breast cancer. Radiology 2004;233(3):830–849.
72. Schott AF, Roubidoux MA, Helvie MA, et al. Clinical and radiologic assessments to predict breast cancer pathologic complete response to neoadjuvant chemotherapy. Breast Cancer Res Treat 2005;92(3):231–238.
73. Nakamura S, Ishiyama M, Tsunoda-Shimizu H. Magnetic resonance mammography has limited ability to estimate pathological complete remission after primary chemotherapy or radiofrequency ablation therapy. Breast Cancer 2007;14(2):123–130.
74. Chen JH, Feig B, Agrawal G, et al. MRI evaluation of pathologically complete response and residual tumors in breast cancer after neoadjuvant chemotherapy. Cancer 2008;112(1):17–26.
75. Kuhl CK, Gieseke J, von Falkenhausen M, et al. Sensitivity encoding for diffusion-weighted MR imaging at 3.0 T: intraindividual comparative study. Radiology 2005;234(2):517–526.
76. Matsuoka A, Minato M, Harada M, et al. Comparison of 3.0- and 1.5-tesla diffusion-weighted imaging in the visibility of breast cancer. Radiat Med 2008;26(1):15–20.
77. Lo GG, Ai V, Chan JK, et al. Diffusion-weighted magnetic resonance imaging of breast lesions: first experiences at 3 T. J Comput Assist Tomogr 2009;33(1):63–69.
78. Belli P, Costantini M, Bufi E, Magistrelli A, La Torre G, Bonomo L. Diffusion-weighted imaging in breast lesion evaluation. Radiol Med (Torino) 2010;115(1):51–69.

Diffusion-weighted Imaging of the Breast: Principles and Clinical Applications

Reiko Woodhams, MD, PhD • Saadallah Ramadan, PhD • Peter Stanwell, PhD • Satoko Sakamoto, MD • Hirofumi Hata, RT • Masanori Ozaki, RT Shinichi Kan, MD, PhD •Yusuke Inoue, MD, PhD

RadioGraphics 2011; 31:1059–1084 • **Published online** 10.1148/rg.314105160 • **Content Codes:** BR OI MR PH

Page 1060
Signal intensity at diffusion-weighted imaging is inversely proportional to the degree of water molecule diffusion, which will be influenced by the histologic structure; in other words, the signal intensity will imply the histologic structure.

Page 1065
The signal intensity at diffusion-weighted imaging becomes lower as *b* value increases, but a higher *b* value emphasizes contrast resolution between various diseases and normal breast tissue. However, an overly high *b* value reduces the overall SNR of the experiment.

Page 1067
The important point is that ADC values can be influenced by which *b* values are applied, a fact that highlights the need for consistent and standardized protocols.

Page 1078 (Figure on page 1079)
Hemorrhage has variable signal intensity and ADC values on diffusion-weighted images (Fig 22). Similarly, hematomas containing intracellular components (intracellular oxyhemoglobin, deoxyhemoglobin, or methemoglobin) show significantly reduced diffusion compared with hematomas containing lysed red blood cells (extracellular methemoglobin) (56,57). Some hematomas have high signal intensity on precontrast T1-weighted images; therefore, T1-weighted images should be evaluated together with diffusion-weighted images to avoid misdiagnosis.

Page 1078
The ADC value after contrast enhancement may not be consistent depending on the diffusion-weighted imaging parameters; therefore, it is recommended that diffusion-weighted images be acquired before contrast enhancement to avoid inconsistency between studies.